Master Thesis

Combined laser ranging and communication on laser terminal CubeCat and TNO's optical ground station

N.W.H. van Tent

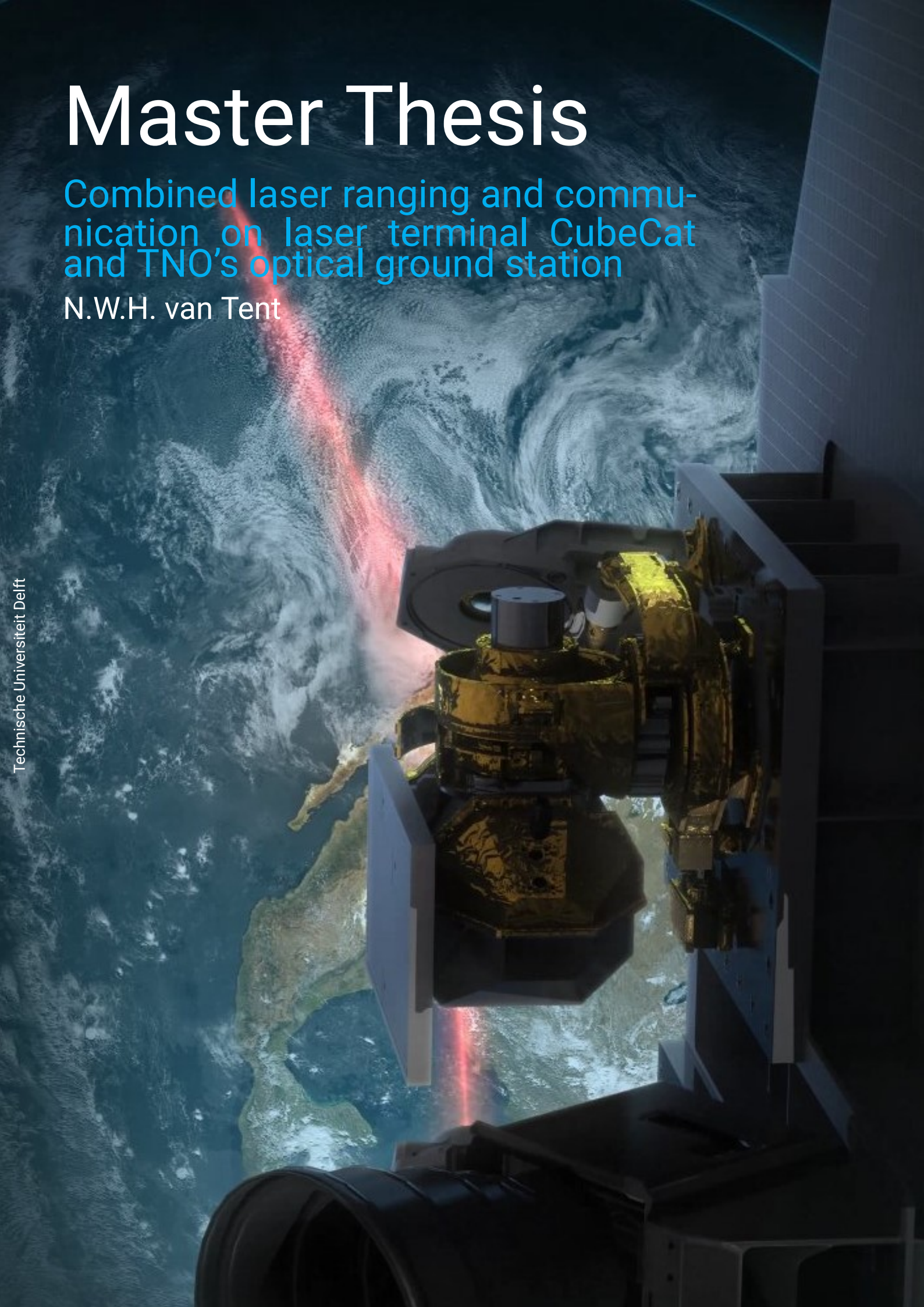

Technische Universiteit Delft

Master Thesis

Combined laser ranging and communication on laser terminal CubeCat and TNO's optical ground station

by

Nina van Tent

Student number:	4383206		
Date:	June 28, 2021		
Committee members:	Dr. ir. D. Dirkx	TU Delft	Supervisor
	Dr. F. Pettazzi	TNO	Supervisor
	Prof. dr. L.L.A. Vermeersen	TU Delft	Chair
	Dr. S. Speretta	TU Delft	Examiner
Cover:	Property of the National Aeronautics and Space Administration (NASA)		

An electronic version of this thesis is available at `https://repository.tudelft.nl/`.

This thesis is confidential and is not allowed to be made public until July 2023.

TU Delft

Preface

The final chapter of my adventure at Aerospace Engineering has approached its end. During the past year I was able to dive into the interesting topics of laser ranging and laser communication. These two industry niches were very new to me and searching for a combined implementation was challenging, but therefore also motivational. Especially because these niches are fast developing and offer a lot of potential for future space missions. Although the thesis has gained me a lot of scientific knowledge, it has also gained me plenty of insight on work ethics. The 'work-from-home' setting has sparked an additional interest for me in topics such as discipline, motivation, productivity and mental-health. I would like to thank Dominic and Federico for their weekly guidance and support. The frequent meetings helped me to stay sharp and motivated during a period of time in which everything is virtual and distant. I would also like to thank TNO for providing me with documentation and the necessary data, and of course for making this cooperation possible.

Nina

Contents

Nomenclature

List of abbreviations

BER	Bit Error Rate
CCSDS	Consultative Committee for Space Data Systems
CSM	Code Synchronization Marker
CW	Continuous Wave
ESA	European Space Agency
FSM	Fine Steering Mirror
GPS	Global Positioning System
ICD	Interface Control Document
IOD	In-Orbit Demonstration
LEO	Low Earth Orbit
LLCD	Lunar Laser Communication Demonstration
NASA	National Aeronautics and Space Administration
NOSA	Norwegian Space Agency
NTP	Network Time Protocol
O3K	Optical On-Off Keying
OGS	Optical Ground Station
OOK	On-Off Keying
PN	Pseudo-random Noise
PPM	Pulse-Position Modulation
PRBS	Pseudo-Random Binary Sequence
PRMS	Peak-to-Root Mean Square
RC	Ritchey-Chrétien
RF	Radio Frequency
RMS	Root Mean Square
RSM	Range Synchroniation Marker
RSS	Root Sum Square
SLR	Satellite Laser Ranging
SNR	Signal-to-Noise Ratio
TLE	Two-Line Element
TOF	Time Of Flight
TUDAT	TU Delft Astrodynamic Toolbox

List of symbols

$\Delta\tau$	Clock error
γ	Obscuration ratio
λ	Wavelength
ρ	Observations (one- or two-way range)
σ	Standard deviation
θ_P	Pointing error angle
$\theta_{1/2}$	Half divergence angle
θ_{BW}	Beam wander angle
B	Bandwidth
C	Clock arc
c	Speed of light
C_D	Aerodynamic drag coefficient
CC	Correlation coefficient
d	Distance
D_R	R_x aperture diameter
g	Correlator quality
G_R	R_x gain
G_T	T_x gain
H	Information matrix
L_P	Pointing loss
L_R	R_x optical loss
L_T	T_x optical loss
L_{ATM}	Atmospheric attenuation
L_{BW}	Beam wander loss
L_{FS}	Free-space loss
L_{SI}	Scintillation loss
L_{SR}	Strehl-ratio loss
P	Covariance matrix
p	Parameters
P_R	R_x received power
P_T	T_x power
P_{apr}	Apriori covariance matrix
p_{out}	Outage probability
P_{REQ}	R_x required power
r_0	Fried parameter
r_c	Beam wander
s	Range

SI	Scintillation index
t	Time
T_i	Integration time
T_{sd}	Symbol duration
V	Voltage
W	Observation weight matrix
W_0	Beam width

List of Figures

List of Tables

Executive summary

The aim of this project was to investigate the feasibility of combined laser ranging and communication between the space-based laser terminal CubeCat and the TNO optical ground station. Combined laser ranging and communication has the potential to expand the capabilities of existing laser communication systems. The range measurements are a valuable asset for the improvement of pointing knowledge and thus pointing accuracy of which the latter is considered as one of the main challenges in optical communication [18]. The first CubeCat demonstrator will fly on-board Norwegian satellite NorSat-TD and is scheduled for launch in 2022[1]. NASA JPL has done research on combined laser ranging and communication with CCSDS compatibility, which they also refer to as telemetry-based ranging [28]. The link protocol of CubeCat will also adhere to the CCSDS optical standards [6][7]. Telemetry-based ranging is a concept mostly known in radio frequency [16]. The concept is less mature in the optical domain but demonstrations have taken place during the Lunar Laser Communication Demonstration Demonstration (LLCD) where centimeter range precision was reached [30]. A CCSDS implementation is, however, not one-on-one compatible with the CubeCat currently being developed because compatibility with O3K encoding is still in the process of being standardized [13].

Telemetry-based ranging with O3K encoding was studied by subjecting an oscilloscope test data set to a correlation technique. By correlating code synchronization markers that are incorporated in the data stream according to the CCSDS standards, the time of flight can be obtained. Two main aspects of this correlation technique that were investigated were correlation ambiguity and range precision. From the data analysis it could be concluded that the correlation size is a dominant factor in the ambiguity of identifying the correlation peak. Precision-wise it was found that the temporal resolution of the data is likely to be the limiting factor. However, it was also found that this temporal resolution induced noise can be reduced to jitter level by increasing the correlation size [3]. Based on this relation, 512-bit and 128-bit synchronization markers were recommended for a 200 kbps uplink and 100 Mbps downlink respectively. This also takes into account the minimum required correlation size to resolve the correlation peak. Through the assumption that timestamps can be traced at a maximum rate of 20 kHz on CubeCat, a maximum downlink data rate reduction of 3% was computed [35].

Besides a study on telemetry-based ranging, it was also investigated in which ranging system it could be placed. These ranging systems include one-way, two-way synchronous and asynchronous ranging. These three ranging systems were compared based on their expected range noise level and orbit estimates. The noise levels of all three ranging systems were found to be in the order of meters for CubeCat and the TNO OGS, which is relatively large compared to the centimeter level noise from the LLCD [30]. However, pre-processing the range measurements before orbit determination could reduce this noise level. The orbit estimates of the ranging systems were compared with a covariance analysis. For this analysis it was important to know that one-way ranging is significantly impacted by stochastic and time-correlated clock noise, which accumulates over time without proper synchronization because timing is done with two different clocks.

The impact of the time-correlated behaviour in one-way range measurements can be reduced with a polynomial estimation on short clock arcs [12]. However, the addition of many extra clock parameters in the estimation complicates isolation of the range signal from the range noise. As a result, crosscorrelations between parameters and formal errors increase. This is a large contrast with two-way ranging where only a single bias term for the clock has to be estimated with an almost negligible effect [12]. For one-way ranging, a formal position error of 274 m was found for a 7-day estimation with 4 state arcs and clock arcs as short as a pass (< 10 min). Apriori information on position, velocity and clock parameters was required to prevent the inverse covariance matrix from becoming singular due to the addition of many clock parameters. The one-way formal position error is a large compared to two-way ranging, whose formal position errors stayed well below 10 m because they only required one clock bias term in the estimation.

[1] NorSat-TD: `https://directory.eoportal.org/web/eoportal/satellite-missions/n/norsat-td`

Based on orbit accuracy, it can be concluded that two-way ranging has a significant advantage over one-way ranging. However, the unmodulated beacon uplink between the TNO OGS and CubeCat makes a two-way ranging implementation currently infeasible, but it is a suggested implementation for future iterations of CubeCat. Although a one-way implementation will not lead to highly accurate orbit solutions, the implementation itself is considered as a valuable demonstration of the telemetry ranging technique for future iterations.

1 Introduction

This chapter introduces the study on combined laser ranging and communication between laser terminal CubeCat and TNO's optical ground station (OGS). First, the scientific relevance of the study is discussed in section 1.1, followed by section 1.2 which contains more background information on CubeCat and the TNO OGS. Section 1.3 and 1.4 elaborate on the concepts of laser communication and laser ranging respectively. The aim of this study is stated in section 1.5, which also includes a supporting research question and sub-questions. Lastly, the report outline is described in section 1.6.

1.1. Scientific relevance

A gradual shift can be observed from radio to optical technology for both ranging and communication systems. For communication purposes, laser systems offer higher data rates and more bandwidth capacity but are also advantageous in terms of power and volume [23]. However, the the atmospheric influence and required pointing accuracy pose stringent requirements on laser communication systems which form the main challenges for this type of communication [18]. The challenge of pointing is where laser ranging could make a difference because the range measurements provide orbit information that could potentially improve the pointing model. In the field of ranging, laser systems are already more mature. The International Laser Ranging Service (ILRS) comprises a large network of laser ranging stations[1]. There are missions that are fully dependent on laser range measurements, such as STARLETTE[2] and LAGEOS[3], but others use the laser ranging measurements in addition to the radio ranging measurements to improve the overall orbit accuracy, such as LRO [5]. Laser ranging and communication systems share many commonalities and have a volume and power advantage over radio frequency (RF) systems. A synergy of the two could therefore be beneficial to a reduction in cost, volume and power [18]. Especially with the shift from large to small satellites in the fields of Earth observation and space exploration, technology synergies are preferred [32]. For example, to reduce volume and/or cost, pointing knowledge on cubesats is often fully based on propagated two-line elements (TLE) instead of an active satellite-based tracker such as GPS [21].

Combined laser ranging and communication could offer a solution to small satellites that are constrained by volume, power or cost [21]. Alternatively, it could expand the capabilities of existing optical communication systems without significant modifications. The latter is considered as the main driver for investigating combined laser ranging and communication capabilities between CubeCat and the TNO optical ground station (OGS). CubeCat, currently being developed by TNO, is an example of a cubesat-sized terminal that will demonstrate in-orbit high-speed satellite-to-Earth laser communication [27]. The aim of this study was to investigate the feasibility of a laser communication and ranging synergy, and more specifically whether such a practical implementation is feasible for CubeCat and the TNO OGS. Section 1.2, 1.3 and 1.4 give more background information on CubeCat, the OGS, and the basic principles of laser communication and ranging.

[1] International Laser Ranging Service: `https://ilrs.gsfc.nasa.gov/about/index.html`
[2] STARLETTE: `https://directory.eoportal.org/web/eoportal/satellite-missions/s/starlette`
[3] LAGEOS: `https://lageos.gsfc.nasa.gov/`

1.2. CubeCat and the optical ground station

CubeCat is a 1U optical communication module that is part of SmallCAT (Small Communication Active Terminal) and developed by TNO. The first CubeCat in-orbit demonstration (IOD) will take place on NorSat-TD, a microsatellite from the Norwegian Space Agency (NOSA). NorSat-TD is scheduled to launch in 2022 into low earth orbit (LEO)[4]. Figure 1.1 and 1.2 show renders of both NorSat-TD and SmallCat respectively. CubeCat is equipped with an O3K (optical on-off keying) modulated laser and will demonstrate a high-speed downlink up to 1 Gbps[20]. Once operational, links will be established repeatedly between the CubeCat terminal and the TNO optical ground station in The Hague.

Figure 1.1: Render of NorSat-TD[4].

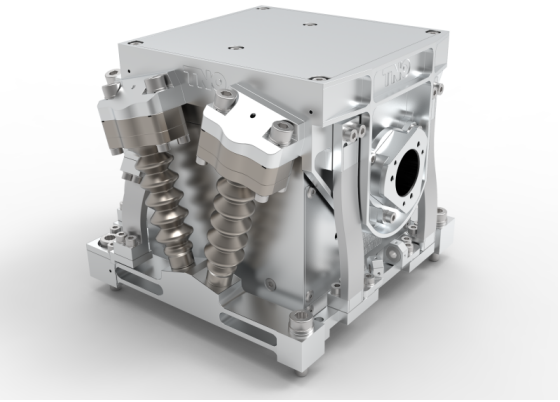

Figure 1.2: Render of SmallCat with integrated laser terminal CubeCat[5].

The TNO optical ground station (OGS) is located at a TNO location in The Hague, The Netherlands[5]. The ground station is not fully operational yet, but is currently undergoing testing. The ground station consists of a Ritchey-Chrétien (RC) alt-az telescope from ASA (Astro Systeme Austria)[6] that is protected by a rotational slit dome as shown in Figure 1.3 [33]. In addition, the ground station will be equipped with a beacon laser to allow for closed-loop pointing, which is discussed in more detail in section 1.3 [35]. Depending on the operational mode and attached instruments, the ground station can track satellites based on reflected sunlight or transmitted laser light. A few parameters of both CubeCat and the OGS are provided as background information in Table 1.1. For additional information on CubeCat and the TNO OGS, or insight in the link budget, it is recommended to consult Appendix A.

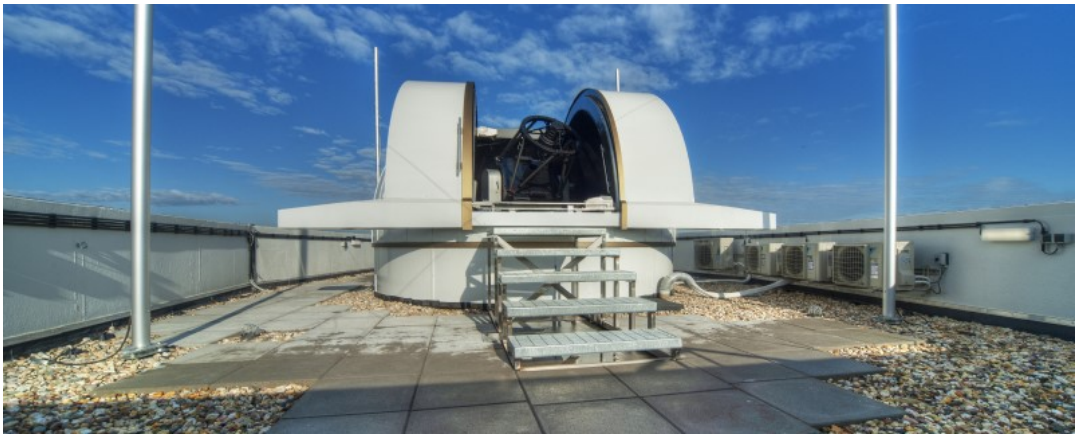

Figure 1.3: TNO optical ground station with an 80 cm Ritchey-Chrétien alt-az telescope[5].

[4]NorSat-TD: `https://directory.eoportal.org/web/eoportal/satellite-missions/n/norsat-td`
[5]SmallCat and TNO OGS: `https://www.tno.nl/en/about-tno/news/2021/1/esa-contract-iod-laser-communication-terminal/`
[6]ASA AZ800 RC telescope: `https://www.astrosysteme.com/products/asa-az800/`

Table 1.1: Specifications of CubeCat and the TNO OGS.

Optical ground station[6]		**CubeCat [20]**	
Aperture diameter	80 cm	Dimensions	96×96×96 mm
Focal ratio	f6.85	Mass	< 1.33 kg
Focus	Nasmyth	Downlink data rate modes	100/300/1000 Mbps
Obscuration by 2nd mirror	41%	Uplink data rate (not used)	200 kbps
Field of view	120 mm	Maximum slant range	1000 km
Tracking precision	1.3 mm RMS/min	Pointing knowledge (from ADCS)	61.9 arcsec (3σ)
Pointing precision	< 20.3 cm RMS	Pointing precision	1800 arcsec (3σ)

1.3. Laser communication

As mentioned in section 1.1, laser communication offers a number of advantages over RF applications. First of all, high data rate links can be established which is suitable for missions with a high scientific data output. Secondly, laser beams are narrow which reduces the footprint on Earth. This makes the application secure for sensitive information. Lastly, laser communication poses less volume and power constraints on the satellite, which is advantageous for satellites with tight constraints on these aspects such as cubesats [18]. An example of cubesats that incorporated laser communication are the AeroCubes developed by Aerospace Corporation as part of the Optical Communication and Sensor Demonstration (OCSD). AeroCube 7B and 7C are examples of 1.5U LEO cubesats that were able to achieve a maximum data rate of 200 Mbps with a 1E-6 BER [26].

Although there are many advantages, there is also a disadvantage. The narrowness of the beams poses stringent requirements on accurate and precise pointing which is considered to be the main challenge in laser communication [18]. Pointing precision is mainly driven by the stability of the surrounding hardware, while pointing accuracy is influenced by how well the laser can be pointed to the provided angles. Then there is also the accuracy of the provided pointing angles themselves which are influenced by pointing knowledge. Pointing knowledge is gathered through a pointing model, which is in turn based on orbit determination and propagation. The latter emphasizes the relevance of enabling simultaneous ranging because it could contribute to orbit determination and propagation, and thus improve the overall pointing knowledge.

As mentioned in the previous section, the links between the TNO OGS and CubeCat consist of a beacon uplink (unmodulated) and a data downlink. Both the uplink and downlink are used for closed-loop pointing. During the acquisition phase, CubeCat will search for the beacon light and will correct its pointing accordingly in a closed-loop configuration during the entire pass. The ground station will implement a similar strategy. Instead of beacon light, the OGS will use part of the light from the data signal for pointing control [35]. It is important to note that the first CubeCat IOD will only consist of a data downlink (i.e. no data uplink). Although there is a possibility to modulate the uplink beacon laser up to 200 kbps, this will at most be used as an acquisition 'handshake', i.e. a moment between ground station and spacecraft in which the communication protocol is confirmed. Any references made in this report towards a data uplink are therefore in the context of future iterations of CubeCat. These references are meant as recommendations and considerations for future development of the CubeCat terminal. The communication protocol of CubeCat and the OGS will adhere to a subset of the Consultative Committee for Space Data Systems (CCSDS) recommended optical communication standards [6][7]. The CCSDS optical standard is relevant for a possible implementation of combined laser ranging and communication, whose concept is introduced in section 1.4.

1.4. Laser ranging

Ranging gives information on distance between the satellite and ground station by measuring the time of flight (TOF). The measurements serve as an input for orbit estimations, which in turn provide information on the position and velocity of the satellite. The quality of these orbit solutions is dependent on the quality of the dynamical model and the quality of the measurements themselves. The latter is of main interest in this study because combined laser ranging and communication changes the baseline technique through which laser range measurements are obtained, compared to traditional satellite laser ranging (SLR). A new technique requires an assessment of the expected precision. Sub-centimeter precisions have been achieved by the SLR

network with LEO orbiting satellites [11]. If combined laser ranging and communication introduces a lower precision compared to SLR standards, it does not necessarily mean that the technique is infeasible. The sub-centimeter level precision of SLR was therefore used as a comparison value for the discussion of the results, instead of a requirement.

In this study three main ranging systems were considered which are one-way, two-way synchronous and two-way asynchronous ranging. In a one-way system the TOF is measured from spacecraft to ground station or vice versa. An example application of one-way laser ranging is LRO whose orbital position could be determined within 30 m with a range measurement precision of 15 cm [5]. In two-way synchronous ranging, the signal is transmitted at the ground station and then retransmitted at the spacecraft to the ground station to obtain a two-way TOF. Two-way synchronous ranging creates a dependency between the uplink and downlink. If this is not preferred a two-way asynchronous system can be implemented in which the one-way TOF is measured in both directions after which the measurements are combined into a single two-way TOF measurement. An example of two-way asynchronous laser ranging is the MESSENGER satellite which obtained measurements with 20 cm precision at 0.2 AU [29]. A more detailed description and underlying principles of each ranging system are given in section 3.1.

To understand the baseline of combined laser ranging and communication it is important to understand what the main differences between laser ranging and laser communication are. In traditional laser ranging, such as SLR, it is common to measure the round-trip time of ultra-short pulses. Repetition rates of 10 Hz are common for picosecond-length pulses [17]. These repetition rates of pulsed ranging are significantly smaller than symbol rates achieved in laser communication. Relevant to this particular example is CubeCat which is being developed to achieve GHz symbol rates [20]. Although pulsed communication systems are power efficient, they are less bandwidth efficient. This makes it a suitable application for deep space applications where signal fading is significantly stronger. However, for near-Earth low-complex systems such as CubeCat it is preferred to go for a simpler laser system and modulation scheme like O3K [13].

The concept of ranging with modulated high-rate signals offers possibilities for simultaneous laser ranging and communication. The Lunar Laser Communication Demonstration (LLCD) on LADEE demonstrated telemetry-based ranging with centimeter level precision using a two-way synchronous system and pulse-position modulation (PPM) [28]. This is a remarkable demonstration because the range quality approaches the precision of SLR. The Consultative Committee for Space Data Systems (CCSDS) provides standards for optical communication [6][7]. NASA JPL has done research on telemetry-based ranging that is compatible with these standards. The disadvantage of the optical standards is that they currently only consider high-photon efficient (i.e. PPM) systems. An O3K variant of these standards is still in development [28]. A disadvantage of NASA's research on telemetry-based ranging is that the proposed ranging system is a two-way ranging system. Two-way telemetry-based ranging is only possible with a modulated uplink and downlink. As mentioned in section 1.3, only CubeCat's downlink is modulated. The 'uplink' is a beacon which is unmodulated. This means that for the current CubeCat one-way ranging is the only feasible option. However, two-way ranging can be considered for future iterations of CubeCat. From this analysis two main research gaps were identified. These research gaps are CCSDS O3K compatibility and one-way telemetry-based ranging which were the focus of the analyses presented in this report in chapter 2 and 3 respectively.

1.5. Research aim

The aim of this study was to investigate the possibilities of combined laser ranging and communication on CubeCat and the TNO OGS. The corresponding research question was: *Can the functionality of TNO's optical ground station and CubeCat be extended to include laser ranging operations?* Additional subquestions were formed to support the answer of the main research question.

1. *Is telemetry ranging based on correlation a feasible option for the CubeCat and OGS link?* This question was answered with a data analysis on the correlation technique which telemetry ranging is based upon. The correlation technique and data analysis are described in chapter 2.
2. *What is the range precision that can be achieved with the clock and timing systems of CubeCat and the OGS?* To answer this question a clock noise budget was set up in subsection 3.3.3.
3. *How does the chosen ranging system affect the accuracy of the estimated orbit?* The impact of a one-way

versus a two-way ranging system was compared with a covariance analysis in chapter 3.

4. *How much does telemetry-based ranging affect the data rate?* Telemetry-based ranging is based on code synchronization markers (CSM) that are part of the data stream, which is explained in chapter 2. This in turn decreases the netto data rate. The impact of this was quantified in section 4.1.
5. *How does a combined laser ranging and communication implementation affect CubeCat and the OGS in terms of hardware and software?* With this question the practical feasibility of telemetry ranging for a one-way and two-way system was determined. The answer to this question is discussed in section 4.3.

The answers to these questions are summarized in the conclusion (chapter 5) of this report.

1.6. Report outline

This section gives an overview of the structure of the report. Chapter 2 describes how a correlation technique can be used to obtain range measurements as a byproduct of the laser communication telemetry. This form of combined laser ranging and communication, or telemetry-based ranging, was subjected to a data analysis to assess its feasibility on CubeCat and the TNO OGS. The data analysis tackled aspects such as CCSDS compatibility, modulation type, correlation size, temporal resolution, and signal-to-noise ratio (SNR). Chapter 3 discusses the type of ranging system in which telemetry-based ranging can be integrated. The essence of clocks and timing for ranging is emphasized in this chapter which has a significant impact on trade-off between one-way and two-way ranging. A covariance analysis was used to assess the expected orbit qualities of the considered ranging systems. The results of both the correlation model data analysis in chapter 2 and the covariance analysis in chapter 3 are presented in chapter 4, as well as a discussion on the recommended practical implementation of combined laser ranging and communication on CubeCat and the TNO OGS. Lastly, the conclusion and recommendations for future work are described in chapter 5 and 6 respectively.

2

Telemetry-based ranging

As stated in section 1.4, pulsed laser ranging is a mature technique where sub-centimeter precisions are reached with SLR [11]. However, it was also stated that for CubeCat and the TNO OGS, this type of ranging is not applicable because their lasers do not operate in the photon starved regime (i.e. pulsed), but instead use OOK modulated continuous waves (CW). This characteristic offers a possibility to incorporate a different ranging technique which is more common in radio ranging. The heritage and current state of this type of ranging is described in section 2.1. This ranging type is based on a correlation technique which is explained in more detail in section 2.2. Lastly, section 2.3 describes the methodology of the data analysis that was applied on the correlation technique.

2.1. Past developments and current state

The essence of correlation-based ranging is that the range measurements are formed as a byproduct of the transmitted telemetry. It is therefore also referred to as **telemetry-based ranging** [16]. To discuss the past developments and current state of this technique, various example applications and demonstrations in the radio and optical domain are described in subsection 2.1.1. Furthermore, a comparative analysis on pulsed and continuous wave signals in the context of the CCSDS optical communication protocols is given in subsection 2.1.2.

2.1.1. Radio versus optical

As mentioned in the introduction of this chapter, the suggested technique for telemetry-based ranging originates from RF applications. Pseudo-random noise (PN) ranging can be considered as an example of two-way telemetry-based ranging. Pseudo-random noise ranging is common in GPS applications[1]. However, as the name says, it is not real telemetry but a repeated pseudo-random bit sequence (PRBS) designed for ranging purposes. The left scheme in Figure 2.1 visualizes a two-way PN ranging scheme. In this scheme it can be seen that the transmitted code at the ground station is retransmitted at the spacecraft, which resembles a two-way synchronous ranging system [16]. The PN ranging scheme in Figure 2.1 (left scheme) needs adjustments to make it compatible with an actual telemetry downlink. NASA JPL has a suggested scheme where the uplink remains a PN range code but the downlink becomes a telemetry stream with intermittent synchronization codewords or code markers. Synchronization code markers (CSM) are small random bit sequences that are repeated in the data stream. The suggested scheme by NASA JPL is two-way asynchronous, meaning that the telemetry downlink is independent of the PN uplink. The corresponding scheme is shown on the right in Figure 2.1. The time measurement that is obtained at the spacecraft is referred to as a 'phase' measurement. This means that there is no separate time measurement for the reception of a PN signal and the transmission of a CSM. Instead, the elapsed phase of the PN sequence at transmission of a CSM is measured. This is only feasible if the PN code is long enough to resolve range ambiguity. A PN repeat period of 0.5 s is a common value for range ambiguity resolvement [16].

[1] GPS PRN codes: `https://www.gps.gov/technical/prn-codes/`

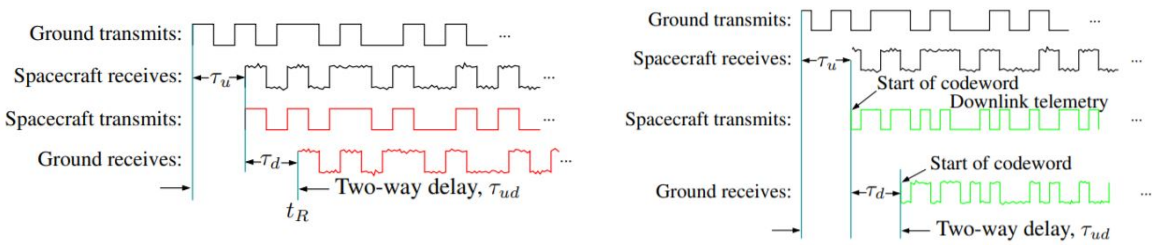

Figure 2.1: (left) Two-way PN ranging by retransmission of the received signal where the time delay is determined on the ground [16]. (right) Two-way asynchronous telemetry-based ranging using a PN uplink and a telemetry downlink with intermittent code synchronization markers (CSM) [16].

As mentioned in the beginning of this subsection, these concepts of ranging originated in the RF domain. However, the concepts are also relevant for the optical domain where this type of ranging is less standard. The Lunar Laser Communication Demonstration (LLCD) on satellite LADEE is a primary example of a telemetry-based ranging demonstration in the optical domain [30]. In this demonstration, centimeter level range precision was reached with two-way TOF measurements with a simultaneous uplink and downlink of 20 and 622 Mbps respectively. TOF measurements were collected at a rate of 20 kHz. The main difference between LADEE and the scheme on the right of Figure 2.1 is that LADEE used a synchronous system with two data links, whereas the scheme depicts an asynchronous system. Synchronous means in this case that the received code markers were aligned with the transmitted code markers [30].

The schemes presented in this subsection are promising but each of them is implemented as a two-way ranging system. For the CubeCat that is currently being developed, this is not an option because the uplink beacon is unmodulated. This is why the impact of a one-way ranging system needs to be investigated. However, a two-way ranging system should not be discarded. If a two-way system shows significant performance improvement, then a modulated beacon can be recommended for future iterations of CubeCat. A comparative analysis of these ranging schemes was made in chapter 3.

2.1.2. Communication protocol

The LLCD is a promising demonstration of combined ranging and communication in the optical domain. However, its modulation type is different from what has been implemented on CubeCat and the OGS. The LLCD used a PPM scheme for its uplink and downlink, while CubeCat uses an OOK modulated CW carrier. High photon efficient (HPE) modulation schemes such as PPM are preferred in complex links that require power efficient beams to close the link budget. These are often missions that are limited by the free-space loss due to the long distance [13]. For less complex systems, such as LEO direct-to-Earth links, a simple scheme like OOK is preferred. An additional advantage of OOK is its bandwidth efficiency compared to PPM [23]. The current CCSDS optical standards however, only cover HPE communication [6][7].

The CCSDS Optical Communications Working Group is aware of the interest from the industry for a low-complexity implementation, and the optical standards are therefore currently being revised to make them compatible with optical on-off keying (O3K). A draft version of the CCSDS optical communications physical layer is already publicly available [8]. When comparing the CCSDS HPE standard with the O3K draft, it can be concluded that there are many similarities. This is a first positive indication that telemetry-based ranging is also compatible with O3K modulation. However, to asses telemetry-based ranging with O3K encoding in more detail a correlation model was set up and a data analysis was performed, which are described in section 2.2 and 2.3 respectively.

2.2. Correlation technique

This section explains the suggested correlation model to obtain TOF measurements as a byproduct of the laser communication data. In subsection 2.2.1, the fundamentals of the model are explained. In subsection 2.2.2, the settings of the simulation model are described in more detail to make the technique reproducible for the reader.

2.2.1. Model principles

The suggested approach to obtain laser range measurements while simultaneously performing laser communication, is based on a correlation technique. A range measurement can be obtained by multiplying the time of flight (TOF) by the speed of light. By correlating part of the received signal with part of the expected transmitted signal (i.e. a CSM) continuously, a time delay equal to the TOF can be obtained. This time delay occurs where the correlation over time peaks which is visualized in Figure 2.2. At this peak the shaded areas, and thus the signals, match. In the remainder of this report, this peak will be referred to as the **correlation peak**. The performance in terms of ambiguity of the correlation process can be evaluated by how well the correlation peak is distinguishable from other (incorrect) crosscorrelation peaks. The example in Figure 2.2 shows little to no ambiguity but this is not always the case. The data analysis in section 2.3 describes how ambiguity in the test data set was analyzed.

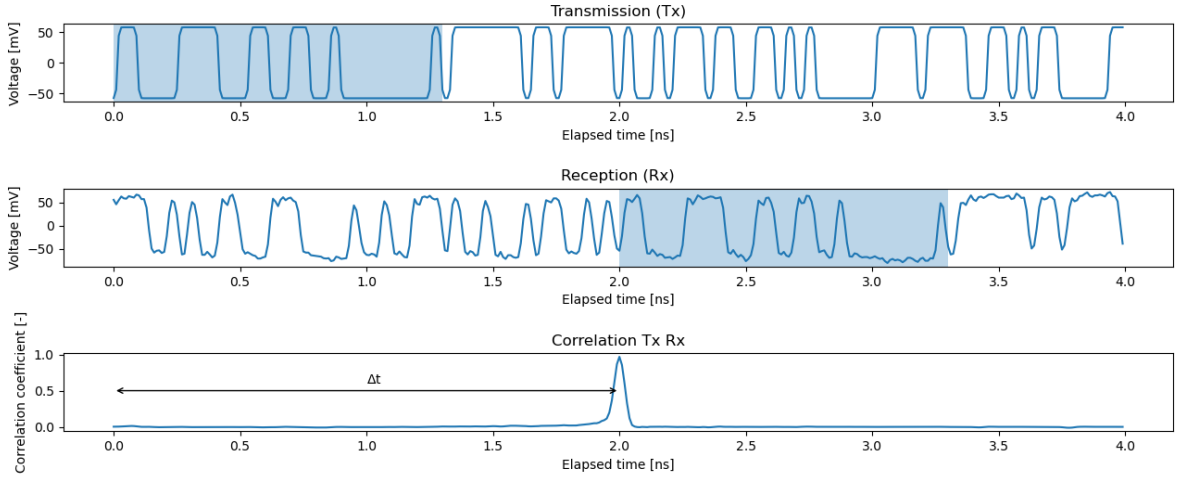

Figure 2.2: Visualization of how the time of flight (Δt) is obtained by continuously computing the correlation coefficient between the expected transmitted (T_x) signal and received (R_x) signal. The shaded parts indicates where the two signals align. (top) Transmitted signal. (center) Received signal. (bottom) Correlation coefficient as a function of time.

There are two main considerations that have to be taken into account in order to make this correlation technique work in real life. First of all, the transmitted sequence and the corresponding timestamps at transmission need to be known at the receiving link end. For two-way synchronous operations such as in RF (left scheme in Figure 2.1) this is rather simplistic because the transmission and reception occur at the same link end (i.e. the ground station) [16]. For two-way asynchronous and one-way ranging the approach is more complex because there is a time measurement both at the ground station and the spacecraft. Thus, implementation-wise the transferability of timestamps has to be taken into account for these types of ranging systems. The feasibility of transferring timestamps with CubeCat lies in the possibility of using CubeCat's tracing file and NorSat-TD's RF downlink [35]. This approach is discussed in more detail in section 4.3. The second consideration was already described in section 2.1, which is that there is currently no CCSDS optical standard available on O3K communication, although it is in development [13]. The data analysis procedure presented in section 2.3 touches upon aspects that were relevant for a preliminary assessment on the feasibility of telemetry-based ranging using O3K modulation.

2.2.2. Model procedure and settings

The input data for the correlation model was obtained from a free-space O3K communication experiment. The data was obtained with an oscilloscope and consists of a voltage waveform. The representativeness of this data is discussed in subsection 2.3.4. In addition, a text file with the repeated PRBS was provided. The step-wise procedure on how to set up the correlation model and use the data is described below.

1. The Tektronix oscilloscope stores the waveform data in a `.wfm` file. To easily read the file into *Matlab* or *Python*, the `.wfm` file was converted to a text file with a *Matlab* script provided by TNO[2]. The text file consists of a column for the observation time and a column for the measured voltage. The script also provides information on the sampling rate.
2. The file was loaded into *Python* in an array. The PRBS file consisting of zeros and ones was converted into the shape of the 'expected' waveform. This basically means that the zeros and ones from the PRBS file were scaled to the voltage amplitudes of the measured waveform. It is recommended that in a future implementation the waveform is scaled to PRBS file, instead of the other way around. The main reason is that it is computationally easier to scale something to ones and zeros than to an amplitude that first has to be calculated. For the test phase this difference was not an issue.
3. A few input parameters need to be provided such as the sampling rate and the data rate. Specific for the correlation technique, a correlation size needs to be provided which resembles the bit-length of a code synchronization marker (CSM). This is an adjustable parameter.
4. The correlation size is used to select a subset of the PRBS file which then becomes the CSM (the shaded area on the top of Figure 2.2). In a loop the CSM is being 'slid' over the waveform with steps of one sample and the correlation coefficient is calculated[3] and stored in an array. This gives results on the correlation coefficient over time as visualized earlier in Figure 2.2 (bottom figure).
5. The location where the maximum correlation coefficient occurs corresponds to the time delay between the transmitted and the received signal, i.e. the time of flight. This delay can be multiplied by the speed of light to obtain the one- or two-way range. If longer parts of the waveform are used then it will be possible to distinguish multiple correlation peaks because the waveform is a repetition of the PRBS.

Besides the correlation technique, other features were added such as a function to create an eye diagram. An eye diagram is a way of visualizing the quality of an electrical signal by overlapping the bits in the analog signal. The result is a figure that looks like an eye as shown in Figure 2.3. The eye diagram is useful to determine certain characteristics of the signal. The jitter was retrieved from the horizontal deviation of the crossings and the rise time from the average time between 10% and 90% of the mean slope [2]. The SNR of this data set was provided (10.6 dB) but can in principle be calculated with the mean voltage levels and the standard deviation of the noise as shown on the right in Figure 2.3.

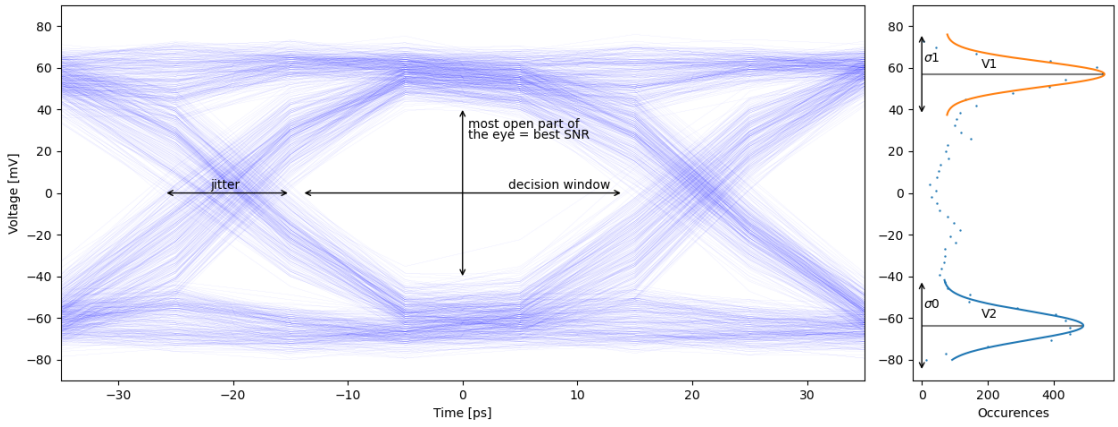

Figure 2.3: (left) Eye diagram of the test data signal. (right) The Gaussian fits represent the distribution of the oscilloscope data points. V_0 and V_1 are the mean zero and one voltage levels with standard deviations σ_0 and σ_1 representing the signal noise.

[2]Matlab script filename: `FU_ReadWFM.m`
[3]The correlation coefficient was calculated with the `numpy.correlate` function

2.3. Data analysis procedure

The data analysis that is described in this section is a preliminary investigation on the feasibility of telemetry-based ranging with O3K modulation. This is needed to verify if the correlation model works and because telemetry-based ranging with O3K encoding has not been demonstrated yet. The data analysis touches upon various factors that drive the performance of the correlation technique. These factors are the correlation size, temporal resolution and signal-to-noise ratio (SNR), which are described in subsection 2.3.1, 2.3.2 and 2.3.3 respectively. As explained in subsection 2.2.2, the experimental data set used for the data analysis was retrieved from a free-space optical communication experiment with an oscilloscope. The data rate (or symbol rate) of this signal is 25 Gbps with a sampling rate of 100 GHz (i.e. 4 samples per bit). The data consists of a PRBS of 2047 bits that repeats itself. The representativeness of the data set is discussed in the subsection on verification of this data analysis (subsection 2.3.4). It should be noted that the subsections below provide a description of the data analysis procedure, but not the results. The actual results of the data analysis are presented in section 4.1.

2.3.1. Correlation size

In section 2.2 it was described how the correlation process works. The ambiguity of this correlation process is primarily driven by the number of samples that are used to compute the correlation coefficients, which is referred to as the correlation or CSM size in this report. It is expected that a small correlation size leads to a situation where the true correlation peak becomes more difficult to discriminate from incorrect crosscorrelation peaks. A larger correlation size should reduce this ambiguity because it has a higher probability of containing a unique pattern. In order to properly quantify the ability to distinguish the correlation coefficient peak $C_{C_{peak}}$ from the crosscorrelations C_{C_i}, the peak-to-RMS ratio (PRMS) [38] was calculated with:

$$\text{PRMS} = \frac{|C_{C_{peak}}|}{\sqrt{\frac{1}{N}\sum_{i=0}^{N} C_{C_i}^2}} \tag{2.1}$$

Where $\sqrt{\frac{1}{N}\sum_{i=0}^{N} C_{C_i}^2}$ is the RMS of N correlation coefficients. The RMS can be considered as a measure of the crosscorrelation noise. If the correlation size increases, the uniqueness is likely to increase as well. As a result, $C_{C_{peak}}$ will increase and the crosscorrelation noise will decrease, and thus the PRMS will increase. The speed at which the PRMS increases for an increasing correlation size will flatten when $C_{C_{peak}}$ starts to approach the limit of 1. To clarify, the PRMS will continue to increase because the RMS in the denominator will continue to approach 0 but the speed of increase will decrease. Thus, the effectiveness of increasing the correlation size becomes less at this point. To visualize this, the PRMS was calculated as a function of the correlation size and presented as part of the overall data analysis results in section 4.1.

In a CCSDS context, the PRMS can be an important factor when choosing the correlation size (i.e. the bit-length of the CSM's). In theory, one could state that a larger correlation size or CSM is always better. However, computationally this would require more time to correlate and in addition, long synchronization markers take up more space in the data stream and thus reduce the data rate more. The desired correlation size is thus a trade-off between the PRMS, computational time and data rate reduction. The computational time could not be properly assessed because it is influenced by the computer details on which the simulation was executed. This is a disadvantage of a high-level programming language such as *Python*. The data rate reduction can be determined by multiplying the CSM size by the repetition rate of the CSM in the data stream. Results of the PRMS calculation and the data rate reduction are presented as part of the overall data analysis results in section 4.1.

2.3.2. Sampling rate

The previous section touched upon the ambiguity of the correlation model and its relation to the correlation size. This section is focused on the range precision that can be obtained with the technique. In subsection 2.2.1, its was stated that a range measurement is a TOF measurement multiplied by the speed of light and that the TOF measurement can be retrieved from the location of the correlation peak. How well the temporal location of the correlation peak can be pinpointed is determined by the temporal resolution of the samples. Excluding interpolation techniques for the moment, it can be stated that the temporal resolution of a sample

is simply equal to inverse of the sampling rate. Each bit needs to be represented by at least one sample so the maximum temporal resolution is therefore equal to the slot width of one bit. The provided oscilloscope data has a symbol rate of 25 GHz and a sample rate of 100 GHz, meaning that each sample has a resolution of 10 ps and that there are 4 samples to describe one bit of 40 ps.

In subsection 2.2.2 it was stated that the correlation coefficient was calculated in a loop with steps of one sample. This implies that the temporal resolution of the correlation coefficients is equal to the temporal resolution of the waveform. This also means that the correlation peak from which the TOF is determined has the same resolution. Thus, the correlation peak of the provided oscilloscope data has a resolution of 10 ps. The temporal resolution of the correlation translates in an uncertainty of the 'true' location of the correlation peak. Through observation the shape of the correlation peak was found to resemble a Gaussian shape. So the true correlation peak is likely to be located within the standard deviation of this Gaussian distribution. From this observation the assumption was made that the precision-induced noise from the correlation has a Gaussian distribution with a standard deviation equal to the temporal resolution.

There are a few approaches to improve the temporal resolution of the correlation peak and thus decrease the corresponding range noise. Two approaches were investigated in this study. The first approach is to apply a Gaussian fitting function on the computed correlation peak and the surrounding correlation coefficients. The peak of the Gaussian fit is considered to be the 'true' peak. The second approach is to apply the correlation over a larger time period, i.e. by increasing the CSM length. Not only does this improve the ambiguity as explained in subsection 2.3.1, it also improves the temporal resolution induced noise because you integrate over a longer period of time. NASA JPL has derived a function that links the sample resolution, correlation size and SNR to the temporal noise [3]:

$$\sigma_t = \sqrt{g \cdot \left(\frac{4T_{sd}^2}{\pi T_i \mathrm{SNR}}\right)^2} \tag{2.2}$$

Where g is dependent on the quality of the correlator and the modulation type. No typical value of g for OOK was provided so its value was assumed to be similar to another binary modulation type, in this case BPSK which has a typical value of 1 [3]. T_{sd} and T_i are the symbol duration (i.e. bit slot width) and integration time respectively. The integration time T_i is equal to the bit-length of the synchronization marker (i.e. the correlation size) multiplied by slot width of one bit. It should be noted that this function was derived in the context of telemetry-based radio ranging. However, since the essence of the correlation technique is similar for both radio and optical telemetry-based ranging, it was assumed that the function holds for optical telemetry-based ranging as well.

Since the symbol duration T_{sd} and correlator quality g are constant, and the SNR can be set to its worst-case value, a minimum integration time T_i, and thus a minimum correlation size, can be found for the maximum desired correlation-induced range noise. This desired maximum is a result of the range noise budget presented in subsection 3.3.3. This subsection started with a description of the impact that the temporal resolution of the communication data stream can have on the range noise, followed by two approaches on how to improve this noise source. The first approach was focused on interpolation which can be applied during post-processing. The second approach was focused on the length of the synchronization markers which has to be determined prior to operations. The results of these two approaches in the context of CubeCat are presented as part of the overall data analysis results in section 4.1.

2.3.3. Signal-to-noise ratio

In subsection 2.3.2 it was stated that a minimum CSM length could be determined if the SNR is assumed to be worst-case. For simplicity it was chosen to base the worst-case SNR on the maximum allowable BER to establish a proper communication link. To compute the SNR, a relation between the modulation type OOK, bit error rate (BER) and SNR was used [2]:

$$\mathrm{BER} = \frac{1}{2}\mathrm{erfc}(\sqrt{\mathrm{SNR}/2}) \tag{2.3}$$

A common value of 1E-6 BER was chosen as worst-case value and by using Equation 2.3, a minimum required SNR of 13.5 dB was calculated [23]. This is also the BER at which AeroCube defined its maximum data rate

[26].

As a final note, the minimum required SNR for the CubeCat links was compared to the SNR of the oscilloscope data set. Their values are 13.5 dB and 10.6 dB respectively. Since the correlation model works on the 10.6 dB oscilloscope data set, it can be assumed that the SNR will not be a limiting factor in the performance of telemetry-based ranging between CubeCat and the OGS. Thus, the oscilloscope test data set is representative in terms of SNR. The representativeness of the test data for other parameters such as the data rate, jitter and rise/fall time are discussed as part of the verification of this data analysis in subsection 2.3.4.

2.3.4. Verification

In this subsection, the correlation model and data analysis are verified. In addition, the representativeness of the used oscilloscope data is argued. Starting with the correlation model and data analysis verification, four sub-analyses were identified which are the correlation model itself and the data analysis steps (correlation size, sampling rate, and the SNR). Table 2.1 summarizes the verification steps of the correlation model and data analysis. In this table *DPOJET*[4] is mentioned which is an application from *Tektronix* for oscilloscope data analysis used by TNO.

Table 2.1: Verification steps of the data analysis procedure on the correlation model for telemetry-based ranging.

Verification step	**Verification**
Correlation technique	
The estimated signal amplitude should approach the amplitude computed by *DPOJET*.	✓A 3.6% difference was determined which can be explained by the fact that only a subset of the data was used (compared to the *DPOJET* output) to decrease the required computational time and memory in *Python*.
The correlation coefficients should have an unambiguous peak for a correlation size equal to the 2047-bit PRBS.	✓See Figure 2.2.
Correlation sample size	
The ambiguity should decrease for an increasing correlation size, thus the PRMS should increase.	✓See Figure 4.1 and 4.2 (part of results)
For a given correlation size, the computation of the PRMS should be repeated multiple times on different locations within the data set. By taking the average PRMS, the behaviour of the plotted PRMS becomes less ambiguous.	✓Figure 4.1 and 4.2 (part of results)
Sampling rate	
The true correlation peak should lie near the computed correlation peak and the two adjacent data points and can be approached with a Gaussian fit.	✓See Figure 4.3 (part of results).
Since the data is a repetition of the PRBS, the correlation peaks should be at equal distance from each other.	✓Picosecond jitter between correlation peaks can be observed with the Gaussian fitting function but these minor differences can be explained by clock performance parameters such as jitter and drift.
The jitter between correlation peaks that can be observed as a results of the Gaussian fitting, can be reduced by increasing the correlation size.	✓See Figure 4.4 (part of results).
SNR	
The eye diagram produced with *Python* should be visually similar to the eye diagram produced by *DPOJET* in order to conclude that the data was correctly imported in *Python*.	✓Minor differences can be explained by the fact that only a subset of the data was used (compared to the *DPOJET* output) to decrease the required computational time and memory in *Python*.

[4]DPOJET from Tektronix: `https://www.tek.com/datasheet/jitter-noise-and-eye-diagram-analysis-solution`

Two main observations were made during the verification of the correlation model and data analysis in Table 2.1. The first being the minor differences observed between the *DPOJET* output and *Python* output. These differences can be explained by the fact that for the data analysis in *Python*, only a subset of the data was used to ensure a time-efficient analysis. The second observation were picosecond differences between correlation peaks after applying a Gaussian fit. These can be explained by clock performance parameters such as drift and jitter.

The remainder of this subsection is devoted to the verification of the data itself by evaluating the representativeness of the data set. The characteristics of the test data set were compared to those that can be expected from the uplink and downlink between CubeCat and the TNO OGS. The comparison of signal characteristics of the oscilloscope signal and the CubeCat up- and downlink is shown in Table 2.2. At a first glance, Table 2.2 shows many differences between the oscilloscope signal and the expected CubeCat/OGS signal. However, it can be argued that the percentage rise time and jitter relative to a bit slot are a better indication of signal shape than the absolute values.

In Table 2.2, it can be observed that the percentages jitter and rise time relative to the bit slot are worse for the test set than what is expected for the up- and downlink between CubeCat and the OGS. This is an indication that the oscilloscope data set actually has a more difficult shape to correlate, with the exception of the percentage rise time of the uplink. Regarding the uplink, it should be noted that this percentage corresponds to the characteristics of the current beacon. This beacon however, is not meant for modulation. If a modulated beacon is indeed installed in the future, it is expected that its percentage rise time will be lower (i.e. improve). To put the percentages into perspective the CCSDS draft recommended standard for O3K communication was consulted. The recommended jitter and rise time percentages of a bit slot are 10% and 30% respectively, so the oscilloscope test set is worse in these aspects than the draft standard [8]. It can thus be concluded that in terms of shape, the test data set serves as a proper worst-case data set.

Table 2.2: Comparison oscilloscope test data set with signal characteristics of the up- and downlink between CubeCat and the TNO optical ground station [34].

Data	**Test set**	**Uplink**	**Downlink**	
Data rate	25 Gbps	200 kbps	100 Mbps	1 Gbps
Bit slot	40 ps	5 μs	10 ns	1 ns
Temporal resolution	10 ps	$\leq$ 5 μs	$\leq$ 10 ns	$\leq$ 1 ns
Jitter	$\approx$ 10 ps	1 ns	20 ps	
Rise time	$\approx$ 20 ps	$<$ 5 μs	$<$ 500 ps	
% jitter of bit slot	$\approx$ 25%	0.02%	0.2%	2%
% rise time of bit slot	$\approx$ 50%	$<$ 100%	$<$ 5%	$<$ 50%
SNR	10.6 dB	13.5 dB (1E-6 BER)	13.5 dB (1E-6 BER)	

Although the shape matters to some extent, the main ambiguity and precision drivers in the correlation process were identified to be the correlation size (subsection 2.3.1) and the temporal resolution (subsection 2.3.2) respectively. The correlation size is an adjustable parameter and therefore not dependent on the test set. The temporal resolution, however, is not an adjustable parameter but the noise it induces can be assessed analytically with Equation 2.2 without the need of a data set. Thus the difference in temporal resolution between the test set and the up- and downlink between CubeCat and the OGS is not an issue in this assessment. Last but not least a note on the SNR values in Table 2.2. As mentioned in subsection 2.3.3, the SNR of the test data set is close, but lower, than the minimum required SNR of the up- and downlink, the test data set is therefore considered as a good representation of a worst-case SNR condition. In short, based on the assessment above it can be concluded that the test data is representative enough for a preliminary feasibility study on O3K modulated telemetry-based ranging through correlation. The next chapter (chapter 3) explains the various ranging systems in which telemetry-based ranging can be implemented.

3

Ranging scenarios

The previous chapter explained the concept of telemetry-based ranging and the underlying correlation model. This chapter describes the ranging systems in which telemetry-based ranging can be applied. A laser range measurement is made by timing the travel time of light from point A to B and multiplying this with the speed of light. This relation emphasizes the importance of timing because a timing error directly translates in a range error. The three main laser ranging systems that were considered in this study are one-way, two-way synchronous and two-way asynchronous ranging. They are described in more detail in section 3.1. The importance of clocks and timing, as well as their relation to the ranging systems, is explained in section 3.2. Lastly, a comparative analysis was done on the various ranging systems to determine the quantitative performance differences between the ranging systems. A covariance analysis was used for this whose procedure is described in section 3.3.

3.1. One-way versus two-way ranging

This section elaborates on the difference between one-way (subsection 3.1.1) and two-way ranging (subsection 3.1.2). An additional distinction is made between two-way synchronous and asynchronous ranging. As mentioned in section 1.3, there is only a modulated downlink on the first CubeCat. This makes one-way ranging currently the only feasible laser ranging option. However, two-way ranging will be treated throughout this report as well because it is viable option for future iterations of CubeCat.

3.1.1. One-way

The essence of one-way ranging is timing the transmission on one end and the reception on the other end of the link. The difference between the timetags produces a time of flight (TOF) measurement. An example of one-way ranging is satellite LRO which used its altimetry detection system to receive pulses from multiple ILRS ground stations that were tagged with sub-nanosecond precision [5][31]. As mentioned in the introduction of this chapter, there is only a downlink between CubeCat and the TNO OGS, and thus the one-way range is considered as a time measurement from satellite to ground in this study. The measured one-way range $\tilde{s}^{(1)}_{BA}$ from satellite (A) to ground (B) can be calculated by multiplying the measured TOF by the speed of light [12]:

$$\tilde{s}^{(1)}_{BA} = c(\tilde{t}_2 - \tilde{t}_1) + \epsilon_{s^{(1)}_{BA}} \tag{3.1}$$

In Equation 3.1 c is the speed of light, $\tilde{t}_1$ and $\tilde{t}_2$ are the measured time at the satellite and ground station respectively. The measured range and time are not ideal because they contain clock errors as explained in more detail in section 3.2. $\tilde{t}$ can therefore be split into the ideal time t and the clock error contribution Δt. Other range errors that are not caused by the clock, such as atmospheric turbulence, are contained in $\epsilon_{s^{(1)}_{BA}}$. By splitting the measured time $\tilde{t}$ into ideal time t and clock error Δt, Equation 3.1 can be rewritten to [12]:

$$\begin{aligned}\tilde{s}^{(1)}_{BA} &= c\Big(t_2 - t_1 + \Delta t_B(t_2) - \Delta t_A(t_1)\Big) + \epsilon_{s^{(1)}_{BA}} \\ &= s^{(1)}_{BA} + c\Big(\Delta t_B(t_2) - \Delta t_A(t_1)\Big) + \epsilon_{s^{(1)}_{BA}}\end{aligned} \tag{3.2}$$

Where $s^{(1)}_{BA}$ represents the ideal one-way range and Δt_A and Δt_B the time dependent clock errors at the satellite (A) and ground station (B) respectively. From Equation 3.2 it can be concluded that the disadvantage of one-way ranging is caused by the clock errors of two different clocks which behave differently from each other. These clock errors have a deterministic and stochastic contribution which is further explain in section 3.2.

3.1.2. Two-way

Two types of two-way ranging are considered in this report. These are synchronous and asynchronous ranging. Two-way synchronous ranging is similar to SLR except that the signal is actively retransmitted instead of passively reflected. SLR or retroreflector ranging was not considered in this study because it is not deemed compatible with simultaneous laser ranging and communication. The fact that the signal experiences free-space and atmospheric losses twice (up and down) makes the ranging system more suitable for pulsed lasers instead of continuous waves. In addition, a retroreflector does not fit in a telemetry-based ranging concept where data has to be transferred from A to B. Two-way synchronous ranging with PN codewords is a common concept in radio ranging, as explained in subsection 2.1.1. Figure 2.1 (left figure) showed how a clean copy of the received PN code is retransmitted by the spacecraft. The New Horizons mission included a PN radio ranging capability and was able to obtain two-way range measurements with a precision of approximately 1 m at a distance of 22 AU [22]. An example in the optical domain is the LLCD whose ranging scheme with synchronization codewords was shown in Figure 2.1 (right figure). With the LLCD centimeter level precision was reached [30].

Two-way asynchronous ranging differs from synchronous ranging in the sense that the uplink and downlink operate independently from each other (i.e. there is no link between the up- and downlink). This means that the two-way range is built-up out of two one-way range observations that are combined into a two-way range during post-processing. During two-way asynchronous radio ranging tests by NASA JPL on the Frontier Radio, nanosecond timing precision was reached [19]. In the optical domain, MESSENGER spacecraft demonstrated two-way asynchronous ranging with 20 cm precision [29]. The measured two-way asynchronous range $\tilde{s}^{(2)}_{BA}$ is equal to [12]:

$$\tilde{s}^{(2)}_{BA} = c(\tilde{t}_4 - \tilde{t}_1) + \epsilon_{s^{(2)}_{BA}} \tag{3.3}$$

Where $\tilde{t}_1$ and $\tilde{t}_4$ represent the measured time upon transmission and reception at clock A, i.e. at the same link end. The first term of Equation 3.6 can be split-up into two one-way ranges and the time between reception of the first ($\tilde{t}_2$) and transmission of the second ($\tilde{t}_3$) one-way range, measured at clock B. Since in this case the ranging is asynchronous, ($\tilde{t}_3 - \tilde{t}_2$) can be negative as well. The resulting equation is [12]:

$$\tilde{s}^{(2)}_{BA} = \tilde{s}^{(1)}_{BA} + \tilde{s}^{(1)}_{AB} + c(\tilde{t}_3 - \tilde{t}_2) + \epsilon_{s^{(2)}_{BA}} \tag{3.4}$$

Where clock A and B correspond to the ground station and satellite respectively. The first three terms from Equation 3.4 can be combined into an ideal two-way range $s^{(2)}_{BA}$ by decoupling the clock errors from the one-way measured ranges $\tilde{s}^{(1)}_{BA}$ and $\tilde{s}^{(1)}_{AB}$ as was done previously in Equation 3.1 and 3.2. The resulting equation contains clock error terms from four timestamps which can be observed in the equation below [12]:

$$\begin{aligned}\tilde{s}^{(2)}_{BA} &= s^{(2)}_{BA} + c\Big(\Delta t_B(t_2) - \Delta t_A(t_1)\Big) + c\Big(\Delta t_A(t_4) - \Delta t_B(t_3)\Big) + \epsilon_{s^{(2)}_{BA}} \\ &= s^{(2)}_{BA} + c\Big(\Delta t_A(t_4) - \Delta t_A(t_1)\Big) - c\Big(\Delta t_B(t_3) - \Delta t_B(t_2)\Big) + \epsilon_{s^{(2)}_{BA}}\end{aligned} \tag{3.5}$$

The second line in Equation 3.5 shows a rearrangement of the terms. From this it can be concluded that two-way asynchronous ranging has a significant advantage compared to one-way ranging. The reason for this is

that for one-way ranging the clock-induced range error is determined by the absolute errors of clock A and B, while for two-way asynchronous ranging the range error is determined by the relative error increases over $t_4 - t_1$ and $t_3 - t_2$ of clock A and B respectively. Equation 3.5 can also be applied to two-way synchronous ranging. With two-way synchronous ranging, there are no time measurements taken with clock B because the retransmission time is assumed to be a constant. This means that the third term in Equation 3.5 becomes obsolete and the resulting equation becomes:

$$\tilde{s}^{(2)}_{BA} = s^{(2)}_{BA} + c\Big(\Delta t_A(t_4) - \Delta t_A(t_1)\Big) + \epsilon_{s^{(2)}_{BA}} \tag{3.6}$$

Two-way synchronous ranging is common in radio ranging but less in the optical domain as mentioned in subsection 2.1.1. The main reason for this is the presence of solar background noise on detectors looking at wavelengths in the optical domain. This could result in accidental retransmissions if the detector cannot distinguish between the transmitted light and background noise [11]. However, telemetry-based ranging, as demonstrated in a two-way synchronous system by the LLCD, does offer potential for this ranging system in the optical domain [30]. In this case retransmission would take place upon reception of a code synchronization marker (CSM) as mentioned in subsection 2.1.2, instead of pulses. A CSM is a long and has a unique pattern compared to a pulse and is therefore less likely to be confused with background noise.

In conclusion, two-way synchronous ranging is advantageous in the sense that the time measurements are taken at the same clock in contrast to a two-way asynchronous ranging. However, two-way asynchronous ranging will still generate significantly better range observations compared to one-way ranging because it only considers error increases over short periods of time. The effect of the one-way clock error on the orbit accuracy compared to the two-way clock error is further described in section 3.2 and 3.3. Although based on this analysis two-way ranging has a better ranging performance compared to one-way, the complexity of the practical implementation should also be taken into account. The suggested implementation for each ranging system is discussed in section 4.3.

3.2. Clock and timing

Timing is an important aspect in laser ranging since a timing error directly translates to a range error. Clocks experience biases and bias instabilities due to e.g. synchronization errors, drift, aging and random noise. In section 3.1, the global time t_i was used in the one-way and two-way range equations, which is a conversion from the measured proper time τ_i. The proper time is the locally elapsed time since a reference time. For simplicity is was assumed that no additional error terms arise in the conversion from proper to global time [12]. Thus it can be assumed that Δt and $\Delta\tau$ are equal. Part of the clock error $\Delta\tau$ (Equation 3.7) is deterministic ($\Delta\tau_d$) and can be modeled with a second order polynomial (Equation 3.8), the other part is stochastic ($\Delta\tau_s$) [12].

$$\Delta\tau = \Delta\tau_s + \Delta\tau_d \tag{3.7}$$

$$\Delta\tau_d = \Delta\tau_d^{(0)} + \Delta\tau_d^{(1)}(\tau - \tau_0) + \Delta\tau_d^{(2)}(\tau - \tau_0)^2 \tag{3.8}$$

In Equation 3.8 $\Delta\tau_d^{(0)}$, $\Delta\tau_d^{(1)}$ and $\Delta\tau_d^{(2)}$ correspond to the bias, drift and aging respectively. Simulating stochastic one-way clock noise in generated observations is a complex process because the noise is correlated in time. It is therefore not as straightforward as a adding a Gaussian noise distribution with independent noise samples. However, when estimating Equation 3.8 for sufficiently small $(\tau - \tau_0)$ clock arcs it can be assumed that stochastic clock noise can be largely removed. A clock arc is a time span over which certain parameters are estimated, in this case clock parameters. The shorter the clock arcs, the easier it becomes to fit a function. If the clock error is short enough, the remaining error will be purely random (i.e. not correlated in time). Figure 3.1 shows the significance of clock arc lengths on the clock error. On the left, the fitting of the polynomial with various clock arc lengths on the total clock error is shown for a lunar orbiter. On the right, the remaining clock error is shown after the polynomial fit is removed. The figure shows that at 28 clock arcs (green lines),

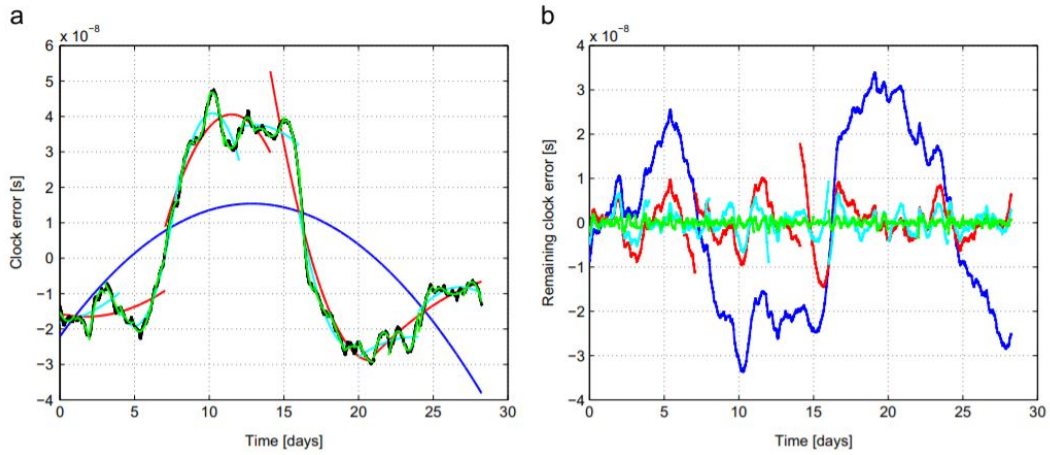

Figure 3.1: (left) The black line represents the clock error propagation on LRO over a 28-day period, the blue, red, cyan and green line represent polynomial estimations for 1, 4, 7 and 28 clock arcs respectively. (right) Remaining clock error after the polynomial estimation [12].

i.e. clock arc lengths of one day, the time-correlated clock noise is largely removed and the remaining error is purely random [12].

Adding short clock arcs is only relevant for one-way ranging. In the comparison of the one-way range equation (Equation 3.2) with the two-way range equations (Equation 3.5 and 3.6), it can be seen that the one-way range is influenced by the difference of two absolute clock errors, while the two-way range is only influenced by the difference of two relative errors over a short amount of time. This means that time-correlated noise is largely removed for two-way range observations and that the remaining bias can be modeled as a constant and a random noise. To conclude, a one-way range estimation can approach two-way range quality if the time-correlated noise can be modelled by adding sufficiently small clock arcs to the parameter estimation. However, there is a limit to the amount of extra clock parameters that can be added to the estimation. Having many parameters in an estimation increases the crosscorrelation between parameters and thus increases the uncertainty by which the state of the space segment, in this case CubeCat, can be estimated. To properly assess the impact of the one-way versus the two-way clock error on the orbit estimates, a covariance analysis was done which is a useful method to compare orbit estimation strategies. Section 3.3 describes the covariance model in more detail.

3.3. Orbit estimation comparison model

Doing a complete parameter estimation for a wide range of input changes is time consuming. The purpose of a covariance analysis is to efficiently compare various estimation strategies without having to do the complete orbit estimation. The estimations that need to be compared are the one-way and two-way estimations. The main difference between these two estimations, as described in section 3.2, is the number of clock parameters that need to be estimated. Adding parameters has an impact on the orbit accuracy. This impact can be quantified with a covariance analysis and this section describes its methodology. The principles of the covariance analysis are described in subsection 3.3.1, followed by a step-wise description of the model in subsection 3.3.2-3.3.4. Finally, the test cases and the verification of the overall analysis was outlined in subsection 3.3.5.

3.3.1. Principles covariance analysis

Covariance matrix P is a matrix that contains the covariances between each possible pair of parameters that needs to be estimated. The number of rows and columns in this matrix is therefore equal to the number of parameters in the estimation. The inverse covariance matrix (P^{-1}) can be calculated with Equation 3.9 [25].

$$P^{-1} = P_{apr}^{-1} + H^T W H \tag{3.9}$$

In which P_{apr} is often a diagonal matrix with apriori covariance knowledge of the estimated parameters. If the inverse apriori matrix is zero, it means that the parameter uncertainty is infinite. H is the information matrix containing the partials $\frac{\delta \text{observations}}{\delta \text{parameters}}$ which describes the linear relation between an observation, in this case range, and the estimated parameters. W is the weight matrix containing the random observation noise. Subsection 3.3.2, 3.3.3 and 3.3.4 are about the setup of the H, W and P_{apr} matrices respectively.

However, a covariance matrix is difficult to interpreted, and thus the matrix is normalized to obtain the correlation coefficients. The correlation coefficients quantify the correlated behaviour between parameters. In other words, whether a change in one parameter influences a change in another parameter. This is an indication of how well the range signal can be isolated from the noise. Another result that can be retrieved from the covariance matrix are the formal errors of the estimated parameters. The formal errors represent the uncertainty by which the parameters of interest can be estimated. With an accurate dynamical model and a good indication of the observation noise, the formal errors will closely match the true errors. The formal errors can be derived from the covariance matrix by taking the square root of the diagonal $\left(\sqrt{\text{diag}(P)}\right)$. Of main interest in this thesis are the differences between the formal errors of the one-way and two-way ranging estimation strategies.

3.3.2. Information matrix (H)

The information matrix H from Equation 3.9 contains information about parameters that cannot be dynamically modelled and are not purely random. This information is given in the form of partial derivatives of the observations with respect to the parameters. As mentioned in subsection 3.3.1, this matrix describes the linear relationship between the observations and estimated parameters. Its size $m \times n$ corresponds to m observations and n parameters. In this case, the observations are either one-way or two-way range measurements. Some parameters are assumed to be constant for the duration of the estimation. Other parameters however, require an arc-wise estimation depending on their expected behaviour, which increases n parameters and thus the number of columns in the information matrix. An arc is a time span over which a parameter is assumed to be constant. In this section there are references to state and clock arcs. A state arc refers to the arc of position and velocity components and a clock arc refers to the arc of clock components, such as bias, drift and aging.

From section 3.1 and 3.2 it could be concluded that **one-way** clock noise is highly stochastic and correlated in time. The deterministic part of the clock error however, can be modeled with a polynomial (Equation 3.8). In combination with short clock arcs to estimate the clock parameters (i.e. shorter than the state arcs), it can be assumed that the time-correlated stochastic noise can be removed and that a purely random clock error will remain. In order to evaluate the impact of many short clock arcs on the formal error of a one-way estimation, clock arcs were added to the original H matrix. The original H matrix describes the linear relationships between the ideal range observations and the parameters. These ideal observations do not contain any clock errors yet and the estimated set of parameters does not contain any clock parameters yet. The vector of estimated parameters $\bar{x}$ for a total of n state arcs that translate to the columns of the original H matrix is:

$$\bar{x} = \begin{bmatrix} x_0 & y_0 & z_0 & \dot{x}_0 & \dot{y}_0 & \dot{z}_0 & \dots & x_n & y_n & z_n & \dot{x}_n & \dot{y}_n & \dot{z}_n & C_D \end{bmatrix}^T \tag{3.10}$$

Here it can be seen that in addition to the position and velocity components, there is a drag parameter C_D in the parameter vector. The two most dominant orbit perturbations of LEO satellites are the gravitational perturbations due to the Earth not being a perfect sphere, and the aerodynamic perturbations in the low-Earth atmosphere. The dynamics of most perturbations can be modeled well, but atmospheric drag is more complex because there is an interaction on molecular level between gas and the spacecraft surface [24]. For this reason the drag coefficient C_D was added to the parameter vector.

Retrieval of the original H matrix was done with the astrodynamical toolbox *Tudat*[1]. *Tudat* has the functionality to simulate dynamics and observations, in this case one- or two-way ranges, based on an initial input which can be an ephemeride or two-line element (TLE). Subsequently, *Tudat* can use the observations to do a parameter estimation. Without going through the entire estimation with multiple iterations, the information matrix H can be retrieved for a generated set of ideal observations. To add the clock arcs, Equation 3.8

[1] TU Delft Astrodynamic Toolbox: `https://tudat.tudelft.nl/`

was used with the assumption that for small time intervals $\frac{\delta\rho}{\delta(c\Delta\tau_d)}$ is linear and therefore equal to $\frac{\Delta\rho}{\Delta(c\Delta\tau_d)}$. Where ρ represents the range observation and $c\Delta\tau_d$ the range error resulting from deterministic clock bias. The resulting clock arc, denoted as C_i, that has to be added to the H matrix is therefore:

$$C_i = \frac{\Delta\rho}{\Delta(c\Delta\tau_d)_i} = \begin{pmatrix} 1 & \tau_{i_0}-\tau_{i_0} & (\tau_{i_0}-\tau_{i_0})^2 \\ 1 & \tau_{i_1}-\tau_{i_0} & (\tau_{i_1}-\tau_{i_0})^2 \\ \vdots & \vdots & \vdots \\ 1 & \tau_{i_n}-\tau_{i_0} & (\tau_{i_n}-\tau_{i_0})^2 \end{pmatrix}_i = \begin{pmatrix} 1 & 0 & 0 \\ 1 & \tau_{i_1}-\tau_{i_0} & (\tau_{i_1}-\tau_{i_0})^2 \\ \vdots & \vdots & \vdots \\ 1 & \tau_{i_n}-\tau_{i_0} & (\tau_{i_n}-\tau_{i_0})^2 \end{pmatrix}_i \tag{3.11}$$

In Equation 3.11, the three columns correspond to bias, drift and aging respectively. The rows correspond to the observations that lie within the time domain of the clock arc. τ_{i_0} and τ_{i_n} are the timestamps of the first and last observation in clock arc C_i. Adding n clock arcs manually to the original H_0 matrix from *Tudat* resulted in the following one-way H matrix:

$$H_{\text{one-way}} = \frac{\delta\rho}{\delta p} = \begin{bmatrix} & & C_0 & 0 & \dots & 0 \\ & & 0 & C_1 & \dots & 0 \\ \mathrm{H}_0 & & \vdots & \vdots & \ddots & \vdots \\ & & 0 & 0 & \dots & C_n \end{bmatrix} \tag{3.12}$$

For **two-way** ranging Equation 3.5 and 3.6 showed that the clock error contribution is only a result of the relative bias increase over a short interval. For a LEO satellite pass the $(t_4 - t_1)$ intervals are in the same order of magnitude (milliseconds) during the entire pass. Similarly, the retransmission intervals $(t_3 - t_2)$ will also be in the same order of magnitude from each other. Looking back at Figure 3.1 it can be seen that the time-correlated stochastic behaviour becomes distinguishable over intervals larger than a day. Since the $(t_4 - t_1)$ and $(t_3 - t_2)$ intervals are much smaller than a day, it can be assumed that time-correlated stochastic clock noise is negligible in the two-way range observation and thus only one clock arc has to be added to the information matrix. In addition, since the $(t_4 - t_1)$ and $(t_3 - t_2)$ intervals are small and nearly constant, it can be assumed that the polynomial clock contribution will be nearly constant as well in all observations. The polynomial clock contribution can thus be modeled as a single parameter over a single arc and therefore the resulting information matrix H becomes:

$$H_{\text{two-way}} = \frac{\delta\rho}{\delta p} = \begin{bmatrix} & & 1 \\ \mathrm{H}_0 & & \vdots \\ & & 1 \end{bmatrix} \tag{3.13}$$

When comparing the one-way and two-way information matrix it can be concluded that the main difference is the number of columns that has to be added to the original H_0 matrix. For a one-way estimation, this is equal to $3\times n$ clock arcs, while for a two-way estimation the clock contribution can be assumed constant based on Equation 3.5 and 3.6. The disadvantage of many extra parameters in the estimation is the increased crosscorrelation between parameters. With a large set of parameters it becomes more difficult to isolate the range noise and thus the crosscorrelation increases. Subsequently, the uncertainty, or formal errors, by which the parameters can be estimated increases as well [11]. The quantitative result of this is described in section 4.2.

3.3.3. Range noise (W)

The weight matrix W in Equation 3.9 is a diagonal matrix and contains information on the purely random noise that the observations contain. The diagonal values of W are equal to the squared inverse of the range noise $(1/\sigma^2)$. In this covariance analysis all range observations that are part of a single estimation are given the same weight. However, a distinction is made between one-way, two-way synchronous and two-way asynchronous range noise. A preliminary analysis was made on the various noise sources that influence the range measurement. Some of these noise sources could be quantified with available information on the TNO optical ground station and CubeCat. The remaining noise sources were quantified based on literature and assumptions. It is important to note that in the noise budgets of the two-way systems, it is assumed that the

beacon uplink can be modulated with a 200 kHz symbol rate [20]. Modulation is not applicable to the current beacon uplink but can be to future iterations of CubeCat. Each noise source was numbered and their respective location of occurrence is visualized in Figure 3.2. Note that the numbered noise sources in Figure 3.2 are not applicable to all ranging systems. Table 3.1 states which noise sources are applicable to which ranging systems.

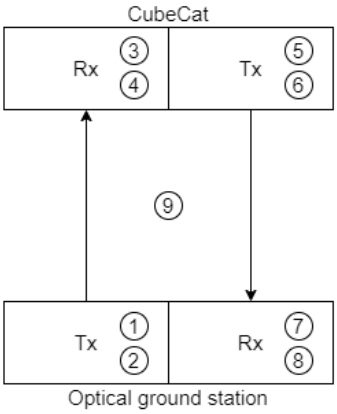

Figure 3.2: Location of occurrence of various range noise sources.

Each numbered noise source in Figure 3.2 was quantified as follows:

1. **OGS GPS time precision (T_x):** The ground station uses a GPS receiver as a reference clock that is synchronized using software synchronization with the NTP server. In this analysis, additional noise sources from the software synchronization process were neglected and instead, the time precision of the reference GPS receiver was considered as the overall precision, which is 6 ns [36].
2. **OGS modulation jitter (T_x):** The CubeCat-OGS ICD describes a 1 ns jitter induced by the T_x oscillator that has a nominal clock rate of 200 kHz [34]. Jitter is caused by short-term frequency changes in the oscillator and is visible in the eye diagram as the horizontal displacement of the crossings (see Figure 2.3 as an example).
3. **CubeCat temporal resolution (R_x):** In a worst-case situation the temporal resolution of a timestamp is equal to the duration of one bit (as explained in subsection 2.3.2). The CubeCat-OGS ICD describes a maximum uplink symbol rate of 200 kHz, which could translate to a resolution of 5 μs (1/200 kHz). In subsection 2.3.2 it was concluded that the temporal resolution translates to a random noise as a result of the correlation model. However, microsecond temporal noise will translate to a few hundreds of meters range noise. This order of magnitude is not desired because it will increase the formal errors significantly. In subsection 2.3.2 two improvements were suggested that allow the temporal resolution induced noise to be reduced to a negligible level by increasing the SNR and/or correlation size. In section 4.1 a quantification of this improvement is presented.
4. **CubeCat GPS time precision (R_x):** This corresponds to the induced noise by the timing precision of the received signal on CubeCat. Literature on GPS timing precisions on cubesats is limited and therefore a comparison of timing precisions for LEO orbits of various commercial space-based GPS receivers was made[2]. This has resulted in a combined value of 40 ns that was assigned to the timing precision of CubeCat.
5. **CubeCat GPS time precision (T_x):** The timing of the received and transmitted signal is assumed to be done with the same GPS timing system. Thus, similar to (4) a 40 ns value was assigned to the timing precision of the transmitted signal on CubeCat.
6. **CubeCat modulation jitter (T_x):** The CubeCat-OGS ICD states a 20 ps jitter induced by the modulation clock that has a clock rate of 1 GHz [34]. As mentioned in (2), jitter is caused by short-term frequency changes in the oscillator.

[2]Reference satellite GPS receivers: `https://gdmissionsystems.com/communications/spaceborne-communications-and-electronics/spaceborne-gps-receivers`

7. **OGS temporal resolution (R_x):** Based on the logic of (3), the lowest specified downlink symbol rate for CubeCat is 100 MHz [20], thus the largest possible temporal resolution is equal to 10 ns (1/100 MHz). Similar to what is mentioned for (3), the temporal resolution induced noise can be reduced to a negligible level based on the suggested improvement presented in subsection 2.3.2.
8. **OGS GPS time precision (R_x):** The timing of the received and transmitted signal is assumed to be done with the same GPS timing system. Thus, based on the same approach as for (1), a value of 6 ns was assigned to the timing precision of the received signal at the TNO OGS [36].
9. **Atmospheric turbulence:** The length of the optical path fluctuates due to atmospheric turbulence which can be observed as range noise. The standard deviation of the path fluctuation however, is not constant during the pass because it is partially dependent on altitude and elevation which vary in time in a deterministic way. Under strong turbulence conditions and a low elevation (i.e. worst-case), the path length fluctuation is sub-centimeter level. Since this is only a small portion of the overall range noise, the time-varying aspect of the path fluctuation is not considered. Instead, the worst-case condition of 1 cm is assigned to all the generated observations [1].

The assessment above is summarized in Table 3.1 and categorized by ranging system. It should be noted that for two-way synchronous ranging there is no value assigned to timing precision on CubeCat because this type of ranging only records timestamps at the ground station. In addition, it can be observed that the temporal resolutions of (3) and (7) have been put in brackets. It is assumed that their contributions become negligible with the suggested temporal resolution improvements described in subsection 2.3.2. The value in brackets is therefore not included in the RSS value.

Table 3.1: Assessment of random noise sources for various ranging systems. Numbers correspond to those in Figure 3.2 and the enumerated list above. Values in brackets can be minimized to a negligible value and are therefore not included in the RSS.

#	Noise source	One-way	Two-way synchronous	Two-way asynchronous
Uplink				
1	OGS GPS time precision	-	6 ns	6 ns
2	OGS modulation jitter	-	1 ns	1 ns
3	CubeCat sample resolution	-	(5 μs)	(5 μs)
4	CubeCat GPS time precision	-	-	40 ns
Downlink				
5	CubeCat GPS time precision	40 ns	-	40 ns
6	CubeCat modulation jitter	20 ps	20 ps	20 ps
7	OGS sample resolution	(10 ns)	(10 ns)	(10 ns)
8	OGS GPS time precision	6 ns	6 ns	6 ns
Other				
9	Atmospheric turbulence	< 1 cm	< 1 cm	< 1 cm
RSS		**40 ns** **12 m**	**9 ns** **3 m**	**57 ns** **17 m**

From Table 3.1 it can be concluded that for one-way and two-way asynchronous ranging, the dominant noise source is the GPS timing precision on CubeCat (40 ns). Since, two-way synchronous ranging does not require timing on the spacecraft, its RSS value is significantly smaller than the other two ranging systems. For two-way synchronous ranging the GPS timing precision at the OGS is the dominant noise source (6 ns). This leads to an order of magnitude difference between the expected two-way synchronous and asynchronous range noise. The RSS values were compared to other applications. The LLCD, a two-way synchronous optical demonstration, was able to retrieve range measurements with centimeter level noise. This is two orders of magnitude smaller than the two-way synchronous case in Table 3.1. This is remarkable for a communication system that does not possess dedicated ranging clocks. The centimeter level noise in the LLCD observations was however, not the noise of the raw measurements (whose value is not provided). The LLCD was able to reduce the range noise to centimeter level by averaging the TOF measurements over 1 s blocks [30]. This could be done because telemetry-based ranging, such as on the LLCD, allows for multiple range measurements per second because there is less ambiguity in matching the transmitted and received time, which is the case for traditional laser ranging systems such as SLR. For orbit determination purposes, this many additional

observations do not contribute to the orbit accuracy because they do not add sufficiently new information in the information matrix H. Thus instead, it would be useful to average the redundant observations into less but more precise measurements. The impact of this noise improvement on the CubeCat-OGS case has not been quantified in this study. It is recommended that this approach is explored in future work of this study, which is also described in the recommendation of this report chapter 6.

3.3.4. Apriori knowledge (P_{apr})

The last matrix from Equation 3.9 to be discussed is the apriori matrix P_{apr}. The problem posed in subsection 3.3.2 was the negative impact of needing many clock arcs for one-way ranging on the formal error and crosscorrelation. Applying apriori information on the estimated parameters can be an effective method of decreasing the correlations when dealing with many parameters. Apriori information sets boundaries on the estimated parameters, and thus the state formal errors, because the estimation is given less degrees of freedom which allows the range signal to be better isolated from the noise. As a result, the correlations are likely to decrease or it prevents the inverse covariance matrix from becoming singular. It should be noted that well-posed problems of which the formal errors are already well below the apriori uncertainty are minimally affected by apriori information. This section elaborates on the apriori values that were used to constrain the state and clock parameters. Assuming open-source TLE's are used for the initial position and velocity input for each state arc, a position and velocity uncertainty can be determined from literature. As a result, the apriori position and velocity uncertainty were set to 500 m and 6 m/s respectively [37]. A 6 m/s uncertainty might be an overestimate because it is based on classic TLE's prior to 2013. However, the way that TLE's are improved has changed over the past years [14].

From what is currently known about the optical ground station and CubeCat hardware, a preliminary estimation could be made on the one-way and two-way clock parameter uncertainties. In subsection 3.3.2 it was concluded from Equation 3.12 that an orbit estimation for one-way ranging requires three clock parameters (bias, drift, aging) per clock arc. The remainder of this section elaborates on the apriori boundaries set on these clock parameters. CubeCat acquisition protocol states that the ground station and CubeCat time are synchronized to approximately 10 ms at the start of every pass [35]. In addition, the documentation states a time drift of approximately 3 ppm during a pass. The quantities of the uncertainty of the drift and aging are not known but there is a possibility of doing a second synchronization at the end of a pass to quantify the uncertainty of these parameters. This second synchronization is therefore strongly recommended for laser ranging operations between CubeCat and the TNO ground station. Based on the limited information available on clock performance, it was assumed that $\Delta\tau_d$ from Equation 3.8 can be determined with a 10 ms uncertainty. The minimum duration of a CubeCat communications pass is assumed to be approximately five minutes when taking into account that the satellite is difficult to track through zenith. This leads to the approximated quantities of 33 μs/s ($\frac{10ms}{5 \cdot 60s}$) for the drift and 111 ns/s^2 ($\frac{10ms}{(5 \cdot 60s)^2}$) for the aging uncertainty. These values are only applicable to the clock parameter uncertainties of a one-way estimation. It should be noted that the drift uncertainty determined through this approach is an order of magnitude larger than the expected mean value of 3 ppm. It is however more likely that the uncertainty is in the same order of magnitude or lower than the mean value. Based on this observation it was taken into account that there is a possibility that each of the clock apriori quantities could be much smaller than initially guessed. To evaluate how much this would impact the estimated parameters, an additional covariance matrix was computed for clock parameter uncertainties that were two orders of magnitude smaller. However, the differences between these 'low' and 'high' uncertainty cases were actually found to be minimal as presented in the covariance results in section 4.2. It should be noted that once CubeCat is operational there is a chance to further characterize the one-way clock parameter uncertainties. The possibility of doing a synchronization at the start and end of the pass may allow further minimization of these uncertainties.

3.3.5. Verification

The verification of the covariance analysis was split into two parts, namely the verification of the model itself and the verification of the model output. The covariance model was verified by reproducing the results from *Tudat* in *Python 3.8*. A verification checklist was set up in Table 3.2 that displays the verification steps in chronological order. It can be observed that the covariance model behaves as expected. Minor differences were observed between the covariance matrices from *Tudat* and *Python*, and consequently between the correlation matrices. It is expected that this is a result of rounding but the difference is considered negligible.

Table 3.2: Verification steps of the covariance model.

Step	Expected outcome	Verification
Information matrix H		
Denormalize H_0 from *Tudat* with the transformation diagonal from *Tudat*, normalize H_0 again but without transformation diagonal.	Normalized H input should be equal to normalized H output.	✓
Add clock arcs to H_0 and check shape of the new matrix H.	Number of columns should be equal to the number of parameters in the original H matrix from *Tudat* plus the number of clock arcs times three (i.e. bias, drift, aging). Number of rows should not change.	✓
Normalize the new matrix H and create heatmap.	Clock arcs should be visible as rectangular blocks of three columns wide in a diagonal fashion. There should be no overlap between these blocks, nor should there be empty columns.	✓See figure Figure 3.3 (right figure)
Observation weight matrix W **and apriori matrix** P_{apr}		
Create W.	Matrix should be diagonal with with values equal to the squared inverse of the range noise. The size of the diagonal should be equal to the number of observations.	✓
Create P_{apr}^{-1}.	Matrix should be diagonal with values equal to the squared inverse of the parameter uncertainty. A zero in P_{apr}^{-1} should correspond to infinite uncertainty. The size of the diagonal should be equal to the number of parameters in the estimation.	✓
Covariance matrix P		
Compute P^{-1} with $(H^T W H)$ using the original H and W from *Tudat*.	The number of rows and columns should be equal to the number of estimated parameters. P^{-1} should not be singular.	✓
Compute P with $(H^T W H)^{-1}$ using the original H and W from *Tudat*.	P should not have negative diaonal values. The computed P should be equal to P from *Tudat*.	✓RSS differences between *Tudat* and *Python* are in the order of 1E-9 therefore considered negligible.
Formal errors and correlations		
Normalize covariance matrix P from the previous step to obtain the correlation matrix. Diagonal correlations correspond to the formal errors.	The computed formal errors in *Python* should be equal to those from *Tudat*.	✓RSS differences between *Tudat* and *Python* are in the order of 1E-10 and therefore considered negligible.

The remainder of this subsection is devoted to the verification of the covariance output. This was done by comparing the output of the covariance model with the expected output for various test cases. For each test case an assessment was made on the expected behaviour of the formal errors and crosscorrelations. How formal errors and crosscorrelations behave in general has been described throughout section 3.3.

The first test case is the impact of the **number of clock arcs** of a one-way system compared to a single clock arc of a two-way system. Based on logic, the addition of many clock arcs and thus extra parameters will lead to high crosscorrelations and formal errors because it becomes more difficult to isolate parameters. The number of clock arcs that was evaluated ranges from one clock arc that covers multiple days to clock arcs with a duration of one pass (< 10 min). Clock arcs of one pass are particularly interesting because of the synchronization that takes place every pass as explained in subsection 3.3.4. Since observations only take place above a certain elevation, the model was constructed in such a way that it automatically removes clock arcs that do not possess any observations to make sure that no empty columns appear in the information matrix H. The impact of adding clock parameters on the correlations can be observed in Figure 3.3. A correlation matrix shows the linear behaviour between parameters. Preferably crosscorrelations between different parameters are low, because otherwise a situation is created in which an error in one parameter influences the error in another parameter as well. On the left of Figure 3.3 a two-way ranging situation can be observed with three position (index 0-2), three velocity (index 3-5), one drag (index 6) and one clock bias (index 7) parameters. On the right a one-way situation is visualized with 7 clock arcs leading to 21 (7×3) additional parameters (index 7-27). It is clearly visible that the correlations increase when clock parameters are added. Not only do the correlations with clock parameters increase, they also increase between the position and velocity parameters themselves (right figure, top left corner). This means for example that an error in position component x will have more influence on the error in components y and z and vice versa, which was less the case for the two-way situation in the left figure.

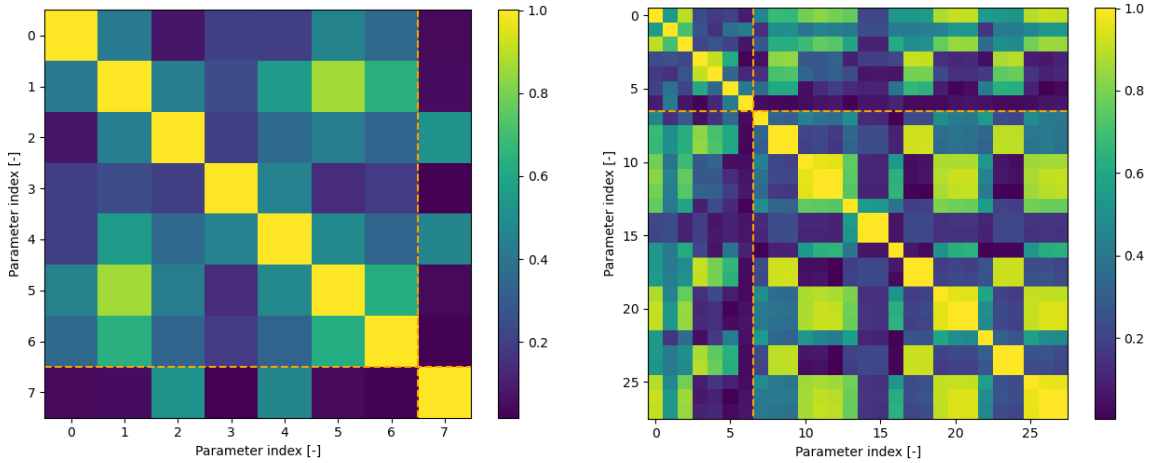

Figure 3.3: Correlation changes based on the number of clock arcs. Both figures show one state arc (index 0-6). Dashed orange lines indicate the starting index of the clock parameters. (left) Two-way with 1 clock arc (index 7). (right) One-way with 7 clock arcs (index 7-27).

The second test case is the impact of **apriori information** of the parameters. Since it is expected that the addition of many clock arcs (e.g. one per pass) for a one-way estimation increases the formal errors and crosscorrelations drastically, it is interesting to see to what extend apriori information can counteract this effect. Similar to the previous test case, the correlation matrices were computed. However, the change in crosscorrelations that could be observed was minimal, as shown in Figure 3.4. In this figure the factor differences between a covariance matrix with and without apriori values can be seen. A few differences can be observed in the covariances of the clock parameters but even these are below 5%. This can be explained by the fact that the formal errors were already well below the provided apriori values. However, the main impact was found to be in the prevention of the inverse covariance matrix from becoming singular. This last aspect will be further discussed in section 4.2.

The third test case is the influence of the **observation noise** (or range noise) in matrix W as described in subsection 3.3.3. A distinction was made between one-way (12 m), two-way synchronous (3m) and two-way

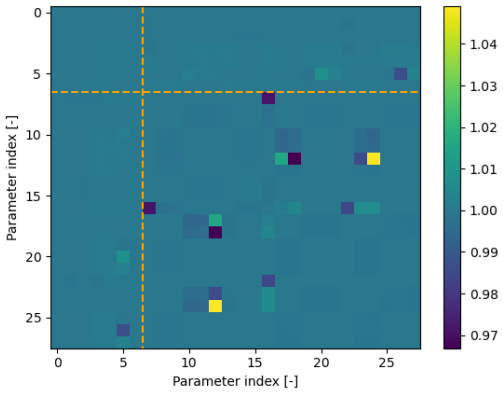

Figure 3.4: Factor difference in the covariance matrices with and without apriori values of a one-way ranging case with 1 state arc (index 0-5), 7 clock arcs (7-27). Dashed orange lines indicate the starting index of the clock parameters.

asynchronous (17 m) range noise. The impact of this differentiation is evaluated with this test case. The two-way ranging cases are the most straightforward to compare because their covariances are structured in the same way but they are computed with different range noise. Figure 3.5 shows that all the covariance values of the asynchronous case are a factor 32.1 higher than the synchronous case. This explains why there is no visible difference in the crosscorrelations of the two cases because if all the covariance values are increased with the same factor than there will be no impact on the normalization of the matrix, and thus the correlation matrix. Since the formal errors are equal to the square root of the covariance diagonal, it can be concluded that the formal errors will increase with a factor 5.7 ($=\sqrt{32.1}$). This factor increase is equal to the factor increase of the noise ($\frac{17m}{3m} = 5.7$), and it can therefore be concluded that the model behaves as expected.

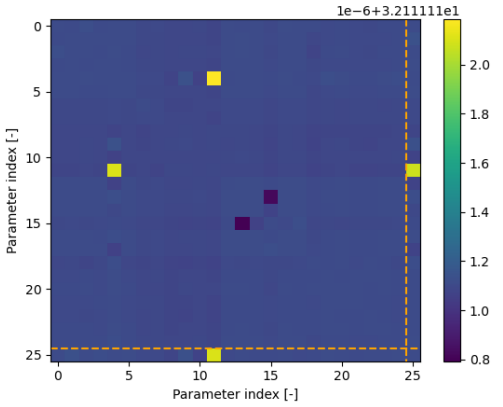

Figure 3.5: Factor increase in covariance values of asynchronous (17 m noise) compared to a synchronous (3 m) ranging case with 4 state arcs (index 0-23) and one clock bias (index 25). Dashed orange lines indicate the starting index of the clock parameters.

The fourth and last test case compares the impact of having **multiple ground stations** that can make range observations. The original use case describes only one ground station (i.e. the TNO optical ground station), so the addition of extra ground stations is hypothetical. It is however, worth to explore because range observations from a single ground station are likely to lead to a large geometrical errors. Based on current developments in the standardization of optical ground stations, it can be assumed that in the near-future networks of optical ground stations will arise and thus the impact of incorporating multiple ground stations is a valid area to investigate. In Figure 3.6 the effect of adding one-way observations of two additional ground stations can be observed with 4 state arcs and 7 clock arcs. In the left figure, which is a situation with one ground station, strong crosscorrelations can be seen between the state (index 0-23) and clock (index 25-45) parameters. In the right figure the impact of three ground station can be seen. Clock arcs were added in a similar fashion for the one-way observations of these two additional ground stations (but are left out of this figure for clarity). The

behaviour that can be observed is that the strong crosscorrelations smoothen out which is likely to be caused by the increase in geometrical information in the information matrix H. However, it can also be observed that other crosscorrelations increase, although softly. This is a result of the additional clock arcs from the two addition ground stations. It was found that this has no negative effect on the formal error because the formal errors of all state parameters decreased, as well as the formal errors of the clock parameters themselves.

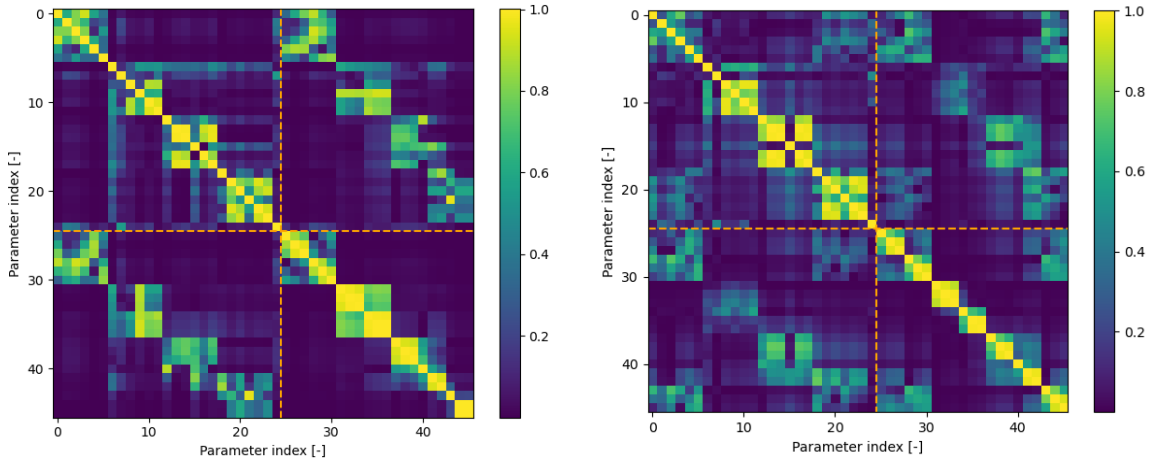

Figure 3.6: Correlation changes based on the number ground stations. Both figures show 4 state arcs (index 0-23) and 7 clock arcs (25-45). Dashed orange lines indicate the starting index of the clock parameters. (left) One-way with 1 ground station. (right) One-way with 3 ground stations.

Table 3.3 shows a concise overview of the test cases described above and the expected behaviour together with a verification checkmark that indicates whether the actual behaviour is in line with the expected behaviour. A quantification of the formal errors for the various test cases is presented as part of the covariance results in section 4.2.

Table 3.3: Test case verification (↑ increase, ↓ decrease, = no change).

Test case	**Formal errors**	**Crosscorrelation**	**Verification**
Adding clock arcs	↑	↑	✓See Figure 3.3
Adding apriori information	↓	↓	✓See Figure 3.4. It should be noted that in this case the change was minimal because formal errors were already well below the apriori uncertainties. The main impact was found to be in the preventing the inverse covariance matrix from becoming singular.
Increasing range noise	↑	=	✓See Figure 3.5. The formal errors increase linearly with range noise.
Adding ground stations	↓	↑ and ↓	✓See Figure 3.6. Strong crosscorrelations decrease but others slightly increase.

4

Results and discussion

Chapter 2 and 3 described the methodologies of the concept study on telemetry-based ranging and the various ranging scenarios in which it can be implemented respectively. The results of these two analyses are summarized in this chapter. Section 4.1 presents the results of the data analysis on the correlation model for telemetry-based ranging. Section 4.2 presents the results of the covariance analysis which compares the various ranging systems. Telemetry-based ranging and the various ranging systems come together in section 4.3 where the suggested practical implementations are discussed.

4.1. Correlation model data analysis

In chapter 2, the principles of telemetry-based ranging and the correlation model were described. In section 2.3 it was explained that the three main factors that influence the correlation are the correlation size, sampling rate and SNR. These factors were part of the data analysis with oscilloscope data whose outcome is presented in this section. Starting with the correlation size, in subsection 2.3.1 it was explained how the correlation size (i.e. length of the synchronization marker) affects the **ambiguity** in discriminating the correlation peak from (incorrect) crosscorrelations. This was tested by repeating the correlation with various correlation sizes. Figure 4.1 shows how the ambiguity improves for larger correlation sizes. Code synchronization markers (CSM) of 16 and 32 bits (top graphs) show relatively high ambiguous behaviour in this O3K data set. It can be argued that small correlation sizes have a less unique pattern and therefore have a higher probability to be accidentally repeated in the overall data stream. From 64 bits and onward, the correlation peak is clearly distinguishable from the correlation noise.

This observation for O3K data of 64 symbols can be compared to the symbol length that is standardized by the CCSDS for high-photon efficient (HPE) systems. For 4-PPM modulation, the CCSDS recommends a CSM length of 24 symbols [6]. That the required symbol length for PPM is smaller than O3K is expected because a PPM scheme fits more than one bit in one symbol. This means that 24 4-PPM symbols actually represent 48 bits which is a better comparison value and also indicates that the required CSM sizes for PPM and O3K can be quite similar. This is a first indication that telemetry-based ranging, whose concepts in literature are mostly based on PPM schemes, is also translatable to O3K. However, it should be verified whether Figure 4.1 is a snapshot moment or whether this behaviour is observed throughout the entire data set. In subsection 2.3.1, the peak-to-RMS (PRMS) ratio was described (Equation 2.1). The PRMS was determined as a function of the correlation size and was calculated multiple times with different bin contents (i.e. different sets of bits with the same size) to get a mean PRMS value (including the standard deviation) which is shown in Figure 4.2. As expected, the mean PRMS increases with an increasing correlation size. The standard deviation is too small to be observed, and thus considered zero. It can therefore be concluded that the behaviour in Figure 4.1 is representative for the entire data set.

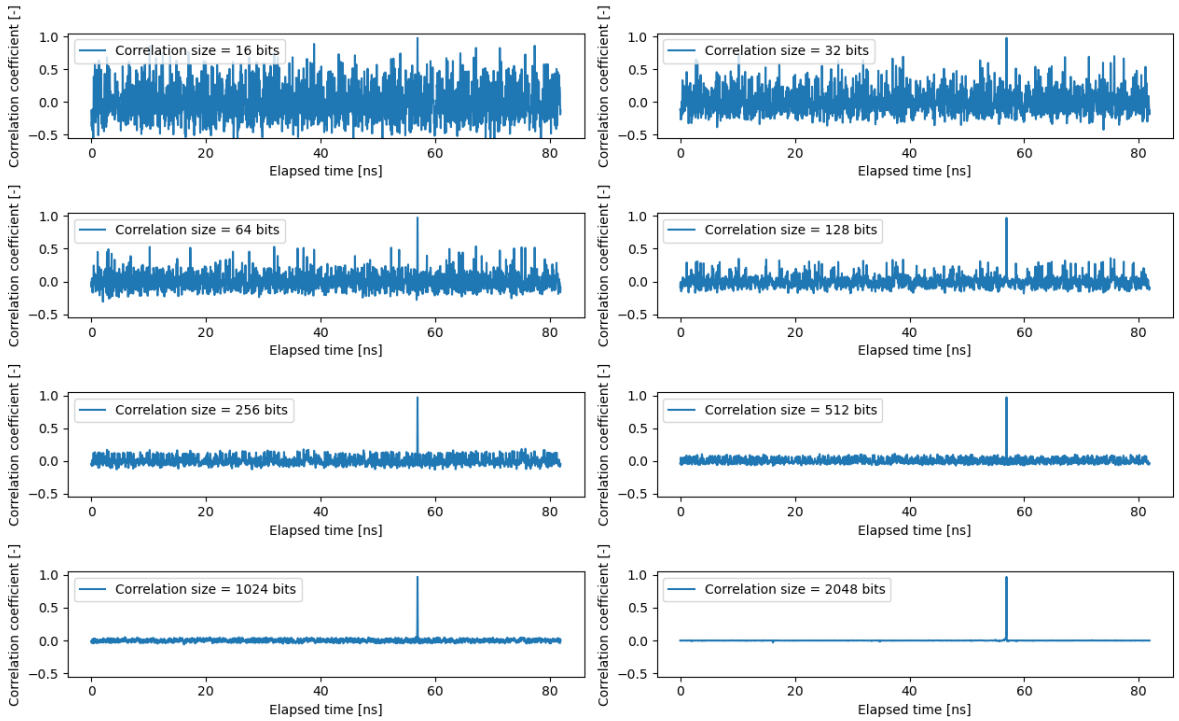

Figure 4.1: Correlation coefficient computed over time for various correlation sizes. Correlation peak becomes more visible for larger correlation sizes.

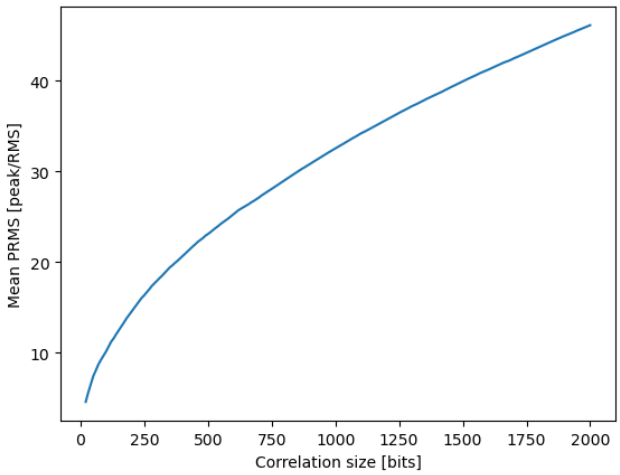

Figure 4.2: The PRMS as a function of the correlation size.

Besides the ambiguity in correlations, the **range precision** that can be obtained through this correlation model was also investigated. In subsection 2.3.2 it was stated that the temporal resolution of the signal data, and thus the resolution of the correlation peak, is equal to the inverse of the sampling rate. In subsection 2.3.2 it was also concluded that the temporal resolution of the correlation peak translates in a random noise in the TOF measurement. This means that if you exclude any interpolation techniques for the moment, the worst-case temporal resolution induced noise is equal to the sample interval of one bit. In this case, a low data rate could become the dominant noise source. To improve this, two suggestions were presented in subsection 2.3.2. The first approach was to apply a Gaussian fit over the computed correlation peak and the adjacent correlation coefficients to determine the 'true' peak more precisely. An example of such a fitting over a correlation peak is shown in Figure 4.3. In this example, there is a 0.5 ps difference between the computed correlation peak and the peak of the Gaussian fit, which can be used to correct the timetag. This is more time efficient than having to interpolate over the entire signal.

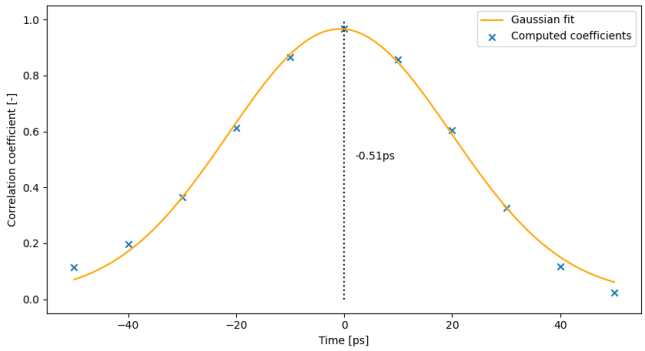

Figure 4.3: Zoom-in on a correlation peak. Example illustration of temporal resolution improvement through Gaussian fitting of the correlation peak. In this example, there is a 0.5 ps difference between the computed correlation peak and the peak of the Gaussian fit.

With this Gaussian fitting method, additional information can be retrieved, such as short-term temporal behaviour by comparing the difference in elapsed time between correlation peaks. Long-term stability can also be assessed by averaging the timestamps of multiple peaks. Figure 4.4 shows the results of short-term behaviour for a small snapshot of the oscilloscope data for several correlation sizes. In addition, a 5-point average was added. If a similar approach is applied on real data of CubeCat it could improve the characterization of random range noise W matrix from Equation 3.9.

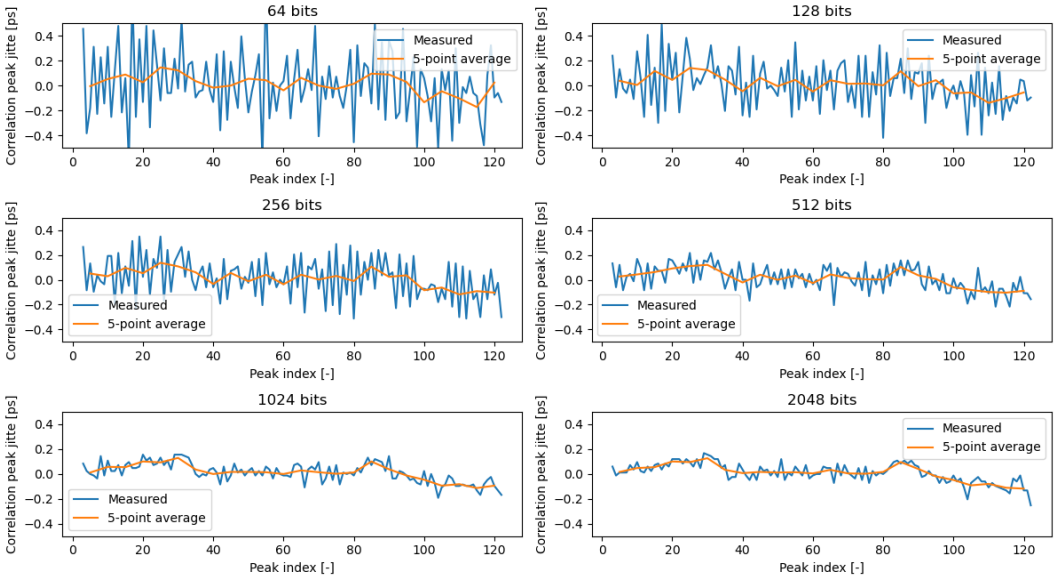

Figure 4.4: Snapshots of short-term behaviour by calculating the time differences between correlation peaks for varying correlation sizes, including a 5-point average.

In Figure 4.4 it can be observed that when the correlation size increases, the noise decreases. This is in line with the analytical expression (Equation 2.2) derived by NASA JPL to determine the time noise from the correlator. In theory the correlation size can be increased to a value where the correlator noise becomes negligible. It is assumed that the correlator noise is negligible when it is smaller than the signal jitter. This assumption, together with a worst-case SNR assumption of 13.5 dB was used to determine the minimum required correlation size for both the uplink (if there is one) and the downlink with Equation 2.2. The minimum correlation size represents the minimum CSM length that delimit the data stream.

Figure 4.5 visualizes Equation 2.2 as a function of SNR and CSM length. To reduce the correlator noise to jitter level on the downlink, a synchronization marker of 32 bits or higher should be chosen. This value is based on the horizontal dotted line which indicates the jitter level and the vertical line which indicates the SNR required for a 1E-6 BER with OOK (defined in this study as the maximum BER). However, it was concluded earlier in this section with Figure 4.1 (top right graph) that a 32-bit correlation size is highly ambiguous and that it is recommended to chose a size of 64 bits and onward. This confirms that the required synchronization marker size should not be chosen solely on range noise improvement but also on correlation ambiguity. For this concept study a 128-bit CSM was chosen for the downlink. For two-way ranging, the uplink needs to be modulated as well. The size of the uplink CSM is chosen in a similar way as for the downlink. From Figure 4.6 it can be seen that a marker of at least 512 bits is required to reduce the correlator noise to jitter level.

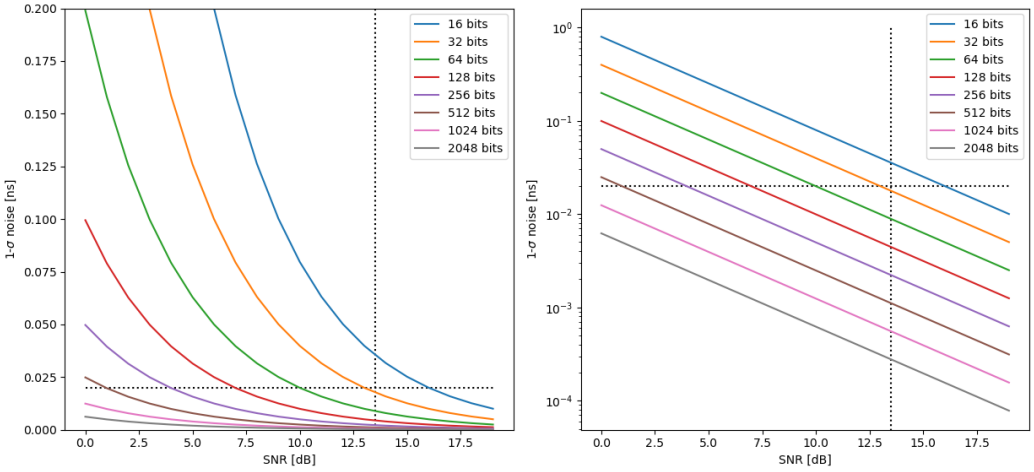

Figure 4.5: Temporal noise improvement for a 100 Mbps downlink. Vertical dotted line: SNR corresponding to 1E-6 BER for OOK. Horizontal line: jitter level (20 ps [34]). (left) Linear scale. (right) Logarithmic scale.

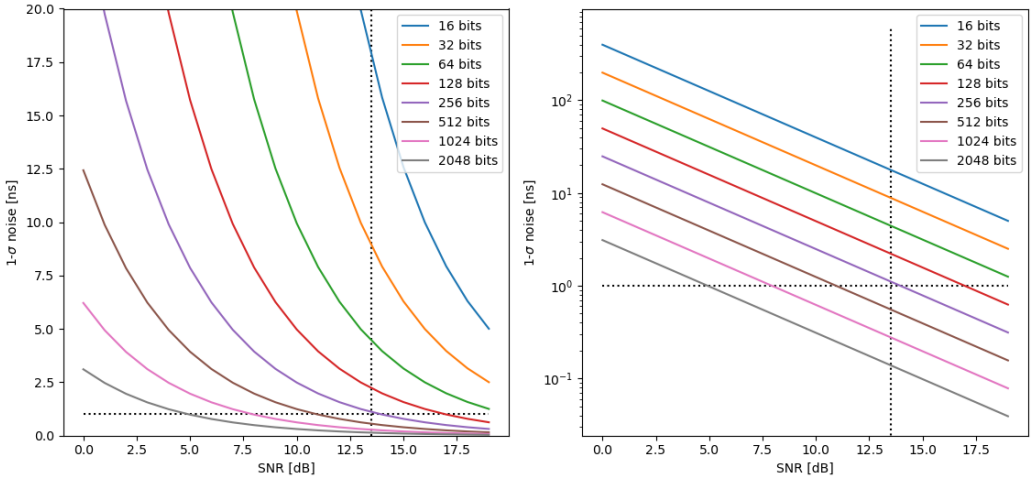

Figure 4.6: Temporal noise improvement for a 200 kbps uplink. Vertical dotted line: SNR corresponding to 1E-6 BER for OOK. Horizontal line: jitter level (1 ns [34]). (left) Linear scale. (right) Logarithmic scale.

Thus, for the downlink and uplink, 128- and 512-bit CSM's were chosen respectively. It should be noted that these values are indicative because the relation from which these values were obtained was written in the context of telemetry-based radio ranging. With an indication of the CSM lengths, the maximum data rate reduction can be derived. Because a CSM is technically also data, the data rate reduction can best be described by 'information rate reduction'. A tracing rate of 20 kHz is described for certain housekeeping parameters of CubeCat [35]. It is assumed that this is also the maximum rate at which timestamps can be stored on the spacecraft. The lowest specified data rate for the CubeCat downlink is 100 Mbps [20]. Tracing 128-bit CSM's at a rate of 20 kHz in a 100 Mbps downlink results is maximum information rate reduction of 3% ($\frac{20kHz \cdot 128bits}{100Mbps}$). The concept of tracing is visualized in section 4.3. In a similar fashion, the maximum information rate reduction on the uplink can be computed. However, it is not expected that the uplink will be used for actual transmission of information and thus there is a likely chance that the uplink stream can be completely filled with synchronization markers. For the uplink a data rate of 200 kbps is described [20]. With a 200 kbps data rate and 512-bit CSM's, a maximum CSM repetition rate of 390 Hz can be achieved.

Two-way synchronous ranging is a special case because the uplink and downlink CSM need to be synchronized. This means that the uplink CSM interval needs to be an integer multiple of the downlink CSM or vice versa [28]. Furthermore, because the CSM is a fixed sequence, there can arise some ambiguity in which transmission timestamp corresponds to which reception timestamp. To prevent this, a different synchronization marker can be added every n number of CSM's. In radio ranging a value of 0.5 s is often used to resolve range ambiguity [28]. Obtaining a range observation every 0.5 seconds is already more than enough. The added value of having more observations is minimal for orbit determination because it does not provide substantial new information to the information matrix H, and thus minimally affects the outcome of the parameter estimation. This means that the time measurements obtained with the CSM's in between these 0.5 s markers can be considered as redundant. In a similar fashion as was done for LLCD TOF measurements, the redundant measurements can averaged over these 0.5 s to remove part of the noise. This is a way of pre-processing the observations before the actual orbit determination. Through averaging the LLCD was able to reduce the noise of the range measurements to centimeter level [30].

4.2. Covariance analysis results

The methodology of the covariance analysis was described in section 3.3. The covariance analysis is based on the assumption of an ideal dynamical model, hence the parameter vector only includes the position, velocity, drag coefficient and clock parameters, because from other parameters it is assumed that they can modeled, as explained in subsection 3.3.2. For this analysis a 7-day range observation set was created with *Tudat* between a 700 km Earth orbiting satellite Terra and the TNO optical ground station in The Hague. Only observations at elevations higher than 25° were generated and the observation interval was 10 s. The Terra satellite was chosen because it is a low-Earth orbiting satellite whose ephemerides are available in the NASA JPL Horizons On-Line Ephemeris System[1]. Four test cases were set up and were described in subsection 3.3.5. As a recap, these test cases are (1) the influence of clock arcs, (2) the influence of apriori knowledge, (3) the influence of range noise, and (4) the influence of multiple ground stations.

The main result of these test cases are formal errors which represent the uncertainty by which a certain parameter can be determined. It is expected that the true errors from a complete orbit estimation will be close to the formal errors of a covariance analysis. The covariance analysis is thus a time-effective way of comparing multiple scenarios without having to go through the complete time-consuming orbit estimation. However, differences between the true and formal errors could arise by mistakes in the dynamical model or when there is a large difference between the range noise provided in matrix W in Equation 3.9 and the actual range noise. The formal error results below are presented as a function of clock arcs. As explained in subsection 3.3.2, clock arcs are the time spans over which the contributions of the clock parameters (bias, drift and aging) are assumed to be constant. This means that for each clock arcs, three parameters are added to the information matrix H. In this analysis a comparison was made between 1, 4 and 7 clock arcs, which translate in a 7-day estimation to 7-, 2- and 1-day clock arcs respectively. Twenty or more clock arcs correspond to clock arcs equal to the duration of approximately one pass (< 10 min). A 7-day range observation set was chosen because smaller sets tend to lead to singular matrices without having added a single clock arc. This can be explained

[1] NASA JPL Horizons web-interface: `https://ssd.jpl.nasa.gov/horizons.cgi`

by the lack of geometrical information in the information matrix due to ranging with only one ground station. An overview of the conditions mentioned above that hold for each test case is shown in Table 4.1.

Table 4.1: Overview of conditions that hold for each of the test cases.

Conditions	**General**	
Estimation duration	7 days	
Observation interval	10 s	
State arcs	1 (≈ 7 days), 4 (≈ 2 days) or 7 (≈ 1 day)	
Conditions	**One-way**	**Two-way**
Clock arcs	1 (≈ 7 days), 4 (≈ 2 days), 7 (≈ 1 day) or ≥ 20 (≈ one pass)	1 (≈ 7 days)

The first test case, as shown in Figure 4.7, quantifies the effect of **adding clock arcs** on the formal error (without apriori information). This is considered to be the main distinction between one-way and two-way ranging when it comes to the parameter estimation. For two-way ranging, the clock error can be estimated with a single bias term, as concluded in section 3.2, while one-way ranging requires an arc-wise estimation of three parameters. The impact is clearly visible in Figure 4.7 as the formal errors for one-way ranging increase rapidly from 7 clock arcs (i.e 1-day clock arcs) onward. The figure shows that the x- and v_x-component are the most dominant factors, especially in the steep incline from 4 to 7 clock arcs. In addition it can be observed that the one-way case with 4 state arcs (blue dotted line) is cut-off after 7 clock arcs. This is caused by singularity of the inverse covariance matrix ($H^T W H$) when more clock arcs are added. Overall, the mean position and velocity error behave similarly in terms of error growth. In addition, the impact of **range noise** between one-way (12 m), two-way synchronous (3 m), and two-way asynchronous (17 m) is also visible in Figure 4.7. These range noise values were determined in subsection 3.3.3. The difference between two-way synchronous and asynchronous is clearly visible as the factor difference between their noise values ($\frac{17m}{3m}$) as described in subsection 3.3.5. One counter-intuitive observation that can be made is that even with zero clock arcs, the one-way case (blue lines) has a larger formal error than the two-way asynchronous case (pink lines) while the latter was given a larger range noise value. When looking at the original information H matrices from *Tudat*, it could be concluded that nearly all the non-zero partial derivatives are a factor 2 larger in the two-way H-matrix compared to the one-way H-matrix which is a logical result of the range being twice as long. Based on Equation 3.9 it can be concluded that the H-matrix in ($H^T W H$) outweighs the impact of the W-matrix (range noise) for two-way ranging, which explains why at zero clock arcs two-way asynchronous (pink lines) has a lower state formal error compared to one-way ranging (blue lines) even though the latter contains less range noise.

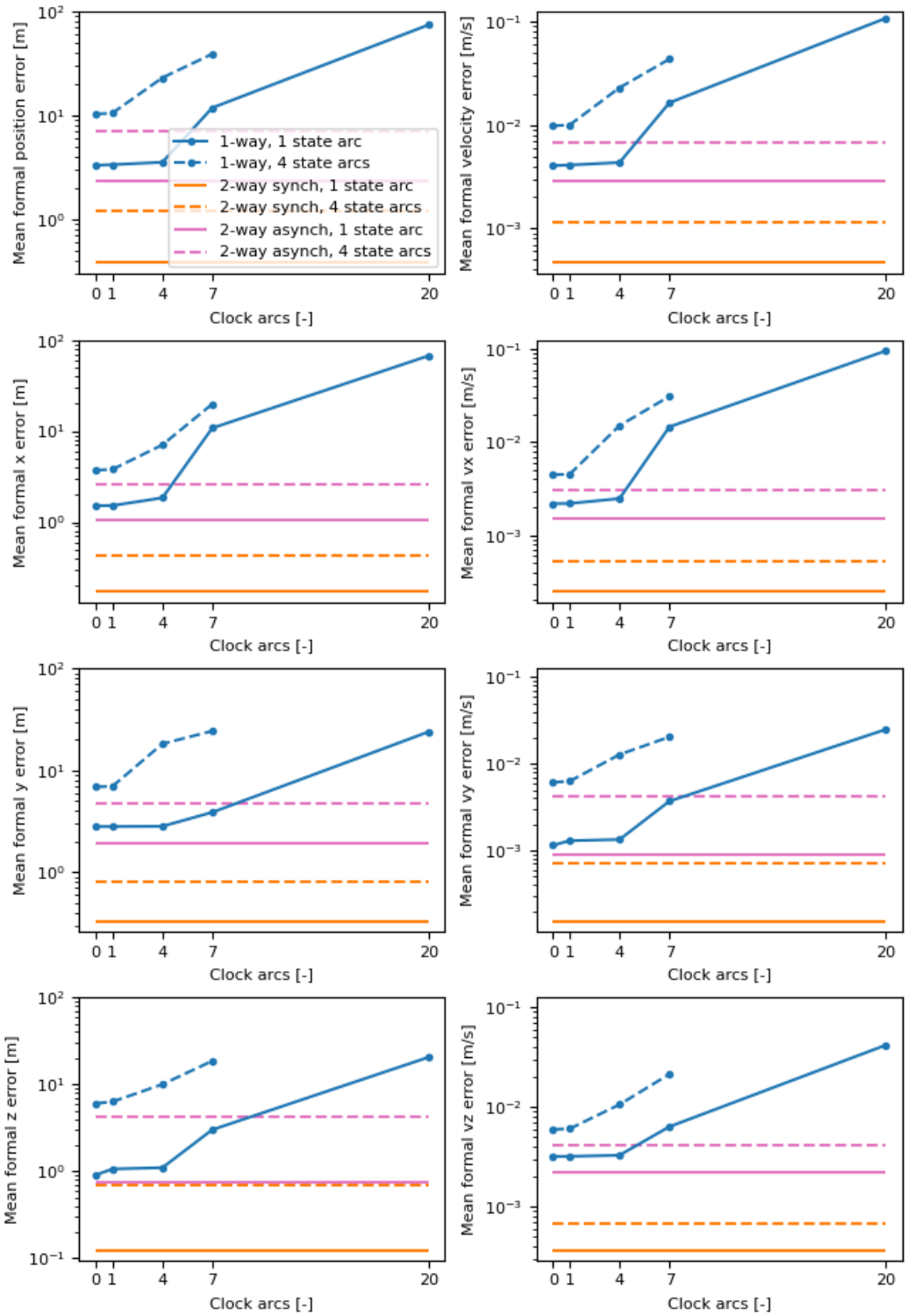

Figure 4.7: Mean formal error as a function of the number of clock arcs. Conditions: 7-day estimation, 10 s observation interval. (left graphs) Position and position-components. (right graphs) Velocity and velocity-components.

The next test case quantifies the effect of adding **apriori information** on the formal errors for one-way ranging. In Figure 4.7, rapid error growth was shown for one-way ranging as a function of the number of clock arcs added. It was also concluded that some cases lead to singular inverse covariance matrices. To counteract this problem and potentially decrease the overall formal errors, apriori information was added on the state and clock parameters. The exact apriori values that were used were stated in subsection 3.3.4. In subsection 3.3.4 it was also stated that two sets of clock apriori values were to be investigated to observe the impact of having 'low' and 'high' clock parameter uncertainties. Figure 4.8 shows the state formal error as a function of clock arcs. The figure clearly shows that the differences between the high and low clock apriori case are negligible, except for a small velocity change for 7 state arcs and clock arcs as short as pass (pink lines). In addition, the overall improvement of formal errors of the case with apriori information (Figure 4.8) compared to the case without apriori (Figure 4.7) is also small. The reason for this can be traced back to the assumption of an ideal dynamical model in which the computation already leads to formal state errors well below the apriori values. The main difference between Figure 4.7 and 4.8 is the presence of singular matrices. In Figure 4.7 only a distinction between 1 and 4 state arcs could be made because every combination of 7 state arcs and any number of clock arcs led to singularity. However, it was found that when adding apriori information the singularity can be prevented as shown in Figure 4.8 (pink lines). The same can be said about the one-way case with 4 state arcs whose state formal errors information could only be computed up till 7 clock arcs (1-day arcs) in Figure 4.7. With apriori information the formal errors could also be computed for clock arcs as short as one pass (orange lines). This is an important aspect because, as discussed in subsection 3.3.4, the apriori clock parameters can best be estimated over one pass due to the clock synchronization command that is scheduled at the start (and possibly also the end) of every pass [35]. So clock arcs of one pass a best representation of reality. Table 4.2 summarizes the results presented in the figures in Figure 4.7 and 4.8 in a table form.

Table 4.2: Overview of the mean formal position errors presented in Figure 4.7 and 4.8.

	Mean formal position error		
State arcs	**1 state arc** (7 days)	**4 state arcs** (2 days)	**7 state arcs** (1 day)
Clock arcs	**Two-way synchronous**		
0	0.4 m	1.2 m	*Singular*
1 (7 days)	0.4 m	1.2 m	*Singular*
Clock arc length	**Two-way asynchronous**		
0	2.3 m	7.1 m	*Singular*
1 (7 days)	2.3 m	7.2 m	*Singular*
Clock arc length	**One-way**		
0	3.3 m	10.3 m	*Singular*
1 (7 days)	3.4 m	10.5 m	*Singular*
4 (2 days)	3.6 m	23.0 m	*Singular*
7 (1 day)	11.8 m	38.9 m	*Singular*
23 (1 pass)	73.9 m	*Singular*	*Singular*
Clock arc length	**One-way + apriori knowledge**		
0	3.3 m	10.3 m	136.0 m
1 (7 days)	3.4 m	10.5 m	138.1 m
4 (2 days)	3.6 m	22.9 m	189.0 m
7 (1 day)	11.8 m	38.8 m	238.1 m
23 (1 pass)	72.9 m	274.0 m	547.1 m

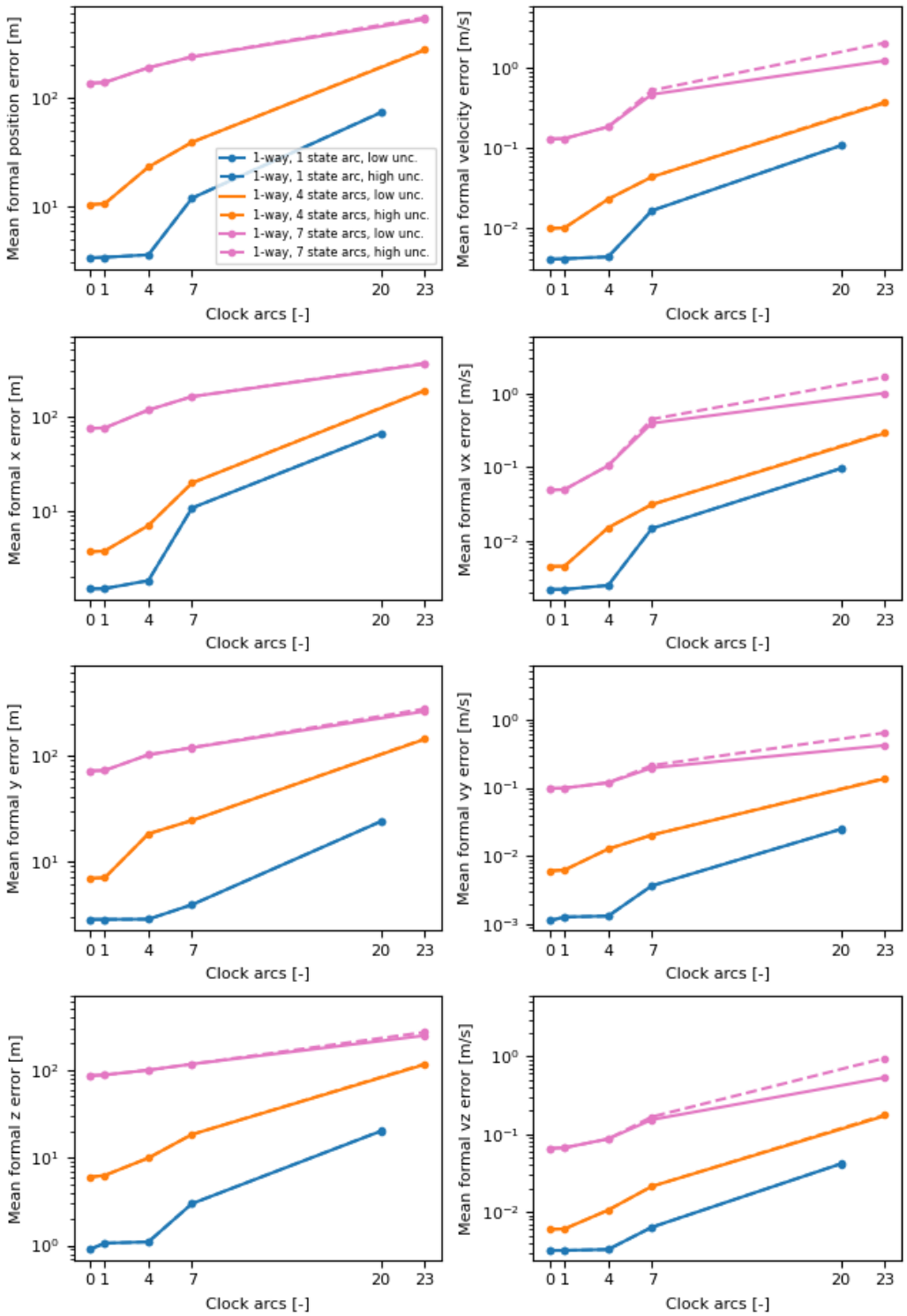

Figure 4.8: Mean formal error as a function of the number of clock arcs including apriori information. Conditions: 7-day estimation, 10 s observation interval. (left graphs) Position and position-components. (right graphs) Velocity and velocity-components.

The last test case that was investigated was the impact of adding range observations from **multiple ground stations** on the one-way formal state error. For this test case, it was assumed that the two additional ground stations provide one-way range measurements under the same conditions as the first ground station. This means that in a similar fashion clock arcs were added to account for time-correlated noise. The resulting formal state errors are shown in Figure 4.9 for an estimation with 4 state arcs. In subsection 3.3.5 it was already discussed and shown that the advantage of additional ground stations is that they smoothen some of the stronger crosscorrelations between state and clock parameters that were part of the case with one ground station. On the other hand, the disadvantage was found to be that some other crosscorrelations actually increased, although softly, which can be accounted to the additional clock arcs for the observations from the other two ground stations. However, it can be concluded that the smoothening of the stronger crosscorrelations has a more dominant effect because the overall formal state errors decreased as shown in Figure 4.9. For the preferred case with clock arcs as short as one pass the formal position error decreased from approximately 274 m to 105 m between one (blue line) and three (orange line) ground stations. The formal velocity error decreased from 0.4 m/s to 0.1 m/s.

In this section the results of four test cases were described. These are influence of clock arcs (Figure 4.7), apriori knowledge (Figure 4.8), range noise (Figure 4.7) and multiple ground stations (Figure 4.9). The influence of clock arcs on one-way ranging was most dominantly visible as a rapid growth in formal error when clock arcs were added. This went up to a point where the inverse covariance matrix ($H^T W H$) became singular and the formal errors could not computed. This problem was solved by adding apriori values on the clock and state parameters. With apriori information and under the conditions of Table 4.1, a formal position error of 274 m was found for a combination of 4 state arcs and clock arcs as short as a day. This is quite a large value compared to the two-way cases whose formal position errors are well below 10 m as a result of only needing a single clock arc. It also approximately an order of magnitude larger than the position error obtained with LRO (30 m) [5]. The most effective way to reduce the one-way formal errors would be to reduce the range noise because it scales linearly with the formal errors. If the one-way range noise could reduced from 12 m to e.g. 1 m (through averaging for example), the formal position error would decrease consequently to approximately 23 m, which is very close to orbital accuracy of LRO. Having clock arcs as short as one day is recommended because of the synchronization command at the start (and possibly the end) of every communication pass provides assurance that apriori clock values can be accurately estimated over these short durations. Table 4.3 gives an overview of the most representative estimation settings from this covariance analysis for each ranging system including the formal errors. In this table it can also be observed that the one-way clock bias uncertainty is approximately two orders of magnitude higher than for two-way ranging.

Table 4.3: Comparison of most representative estimation strategies for a 7-day estimation with 4 state arcs.

	Two-way synchronous	**Two-way asynchronous**	**One-way**
Clock arc length	7 days (1 arc)	7 days (1 arc)	1 pass
Apriori knowledge	No	No	Yes
Mean formal error			
Position	1.2 m	7.2 m	274.0 m
Velocity	0.001 m/s	0.01 m/s	0.36 m/s
Bias	0.6 ns	3.4 ns	392.7 ns
Drift	NA	NA	3.4 ns/s
Aging	NA	NA	14.5 ps/s^2

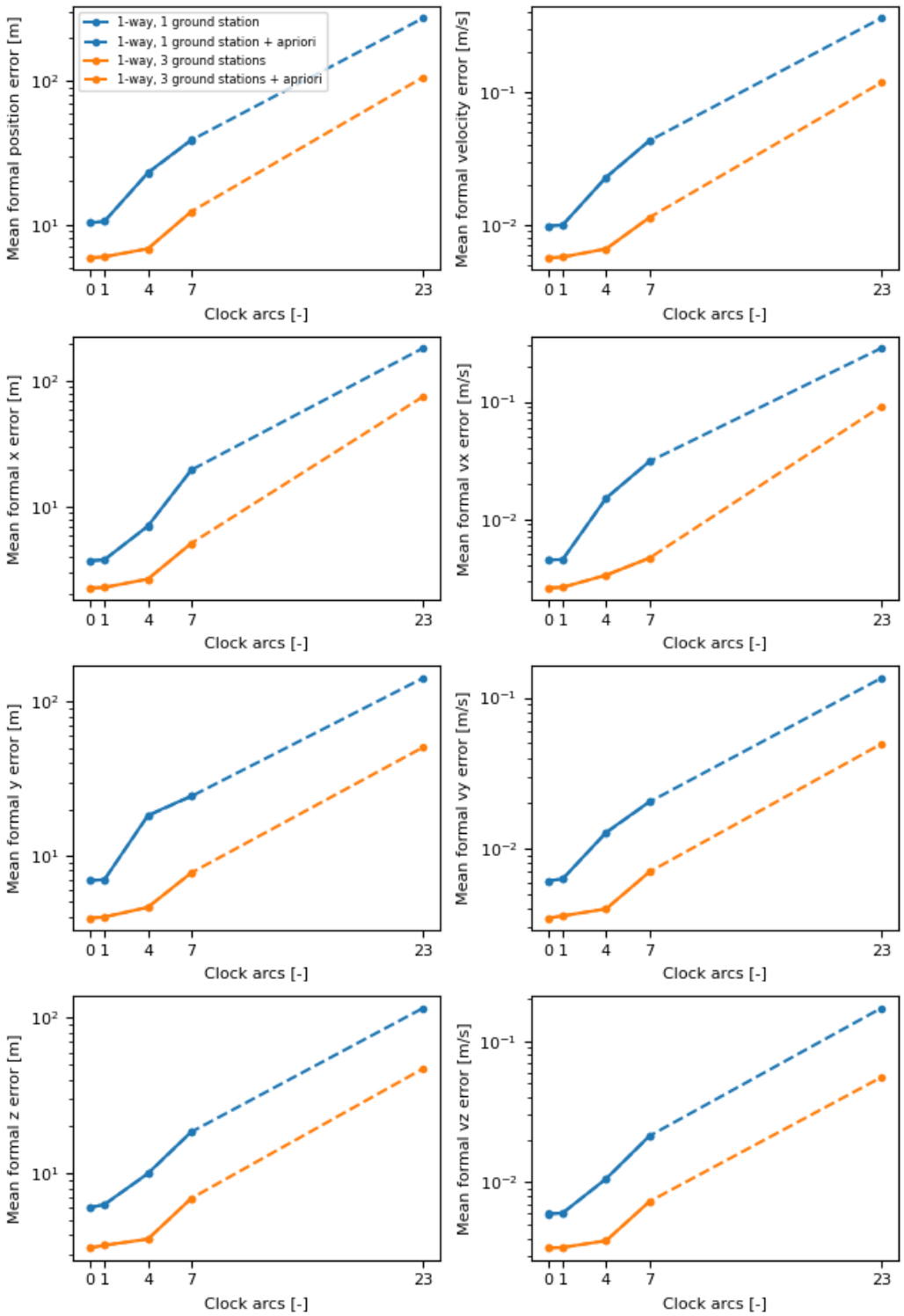

Figure 4.9: Mean formal error as a function of the number of clock arcs for one versus three ground stations. Conditions: 7-day estimation, 10 s observation interval. (left graphs) Position and position-components. (right graphs) Velocity and velocity-components.

Although the formal errors are expected to be near the true errors, there are certain aspects that could increase the difference between the two. The true error will be larger if:

- The dynamical model does not account for certain effects. To decrease this impact, a few additional parameters could be added to the estimation. However, it was stated earlier in subsection 3.3.2 that perturbations in LEO can be modeled quite well except for the aerodynamic drag which was already taken into account in the parameter vector of this covariance analysis.
- The range noise is larger than the values given in the W-matrix. In chapter 6 a recommendation is given on range noise improvement through averaging, as well a recommendation on the overall improvement of the quantification of the noise.
- There are time-correlated noise artifacts over periods less than the duration of one communication pass ($\leq$ 10 min). If this is the case then it is still difficult to predict whether this error will be dominant enough to impact the true errors. However, the automated clock synchronization command at the start of each communication pass provides confidence that if these artifacts do translate to the true errors, the impact will be marginal.

Section 4.3 combines the telemetry-based ranging results from section 4.1 with results on the various ranging systems from this section to provide an outlook on the possible implementations on a short- and long-term.

4.3. Discussion on implementation

This section describes the practical implementation of the one-way and two-way ranging scenarios. The compatibility with the CCSDS optical standard is a point of focus in this case. In the previous sections it was concluded that one-way ranging is currently the only feasible ranging system because there is no modulated uplink. However, the benefit from a two-way ranging system in terms of orbit accuracy was clearly visible in section 4.2 and is therefore recommended for future iterations. It is therefore that this section has been split up in a short-term and long-term outlook on the implementation in subsection 4.3.1 and 4.3.2 respectively. For each suggested implementation, a systems engineering block diagram is provided. Even though there is a significant improvement in orbit accuracy with two-way ranging, it is argued whether the impact of its implementation weighs up against its benefit.

4.3.1. Short-term outlook: one-way ranging

Complexity of a one-way ranging implementation lies in the transferability of timestamps recorded on the spacecraft. Figure 4.10 shows a block diagram that illustrates how the timestamps are retrieved on the spacecraft to obtain a time of flight measurement. In the 'transmitter' block on CubeCat it can be seen that the code synchronization markers or CSM's, together with the data, are used to create CCSDS transfer frames as described in detail by the CCSDS optical standard [6]. The transmission of a CSM should trigger the timing system to create a transmission timestamp, which is then saved in a tracing file. These tracing files are used for housekeeping data and other CubeCat telemetry (including timestamps) and can be transferred via the optical link during the pass or alternatively via a radio link at a later stage. The latter alternative is shown in the block diagram. At the RF ground station, the T_x timestamps can be retrieved from the received tracing file. Moving onto the receiver side of the optical ground station. Here it can be seen how the downlink signal is detected by a detector that is connected to an oscilloscope. The output of the oscilloscope, as shown in the 'post-processing' block, will be the digitized electrical waveform. This has the same format as the waveform used for the data analysis in section 2.3. In fact, the full post-processing block follows the correlation model presented in section 2.2. The data from the oscilloscope can be correlated with a local copy of the CSM's to retrieve the R_x timestamps. Together with the T_x timestamps, a TOF measurement can be obtained that serves as an input for the orbit estimation.

The blocks depicted in orange in Figure 4.10 represent inputs/outputs and action items that have to be added to the existing infrastructure. The impact of these additions is discussed below:

- It can be observed that a large part of the orange blocks can be placed in the 'post-processing' block of the ground segment. This is convenient because a post-processing block has no impact on a system level on CubeCat and the OGS.
- On the transmitter side of CubeCat, synchronization codewords or CSM's have to be added to the CCSDS transfer frames. This procedure is standardized by the CCSDS optical standards so no significant system impact is expected here.
- Upon transmission of the CCSDS transfer frames on CubeCat, timestamps have to be recorded. A deeper understanding of CubeCat's mechatronics is required to determine whether the current system already does this kind of recording. Otherwise, a trigger has to be created that connects the transmitter to the clock and timing system.

From this analysis it can be concluded that most of the infrastructure needed for one-way telemetry-based ranging is already there, which is convenient. The performance side of one-way ranging however, is less favorable. In section 4.2 it was found that for a 7-day estimation with 4 state arcs and apriori information, a formal position error of 274 m was found for clock arcs with a time span of one satellite pass (< 10 m). This is two orders of magnitude larger than the formal positions errors of the two-way ranging systems which do not have to deal with time-correlated clock errors. However, the automated clock synchronization command of the ground station and CubeCat clock at the start (and possibly end) of a pass gives a promising outlook on the determination of tight apriori boundaries, as explained in subsection 3.3.4 [35]. Further reduction of the formal errors could be achieved by minimizing the range noise. The range noise for one-way ranging between CubeCat and the OGS was estimated in subsection 3.3.3 to be approximately 12 m. In section 4.2 it was argued that if the one-way range noise could be reduced (through averaging for example) to e.g. 1 m, the formal position error would approach the error of one-way application LRO ($\approx$ 30 m) [5].

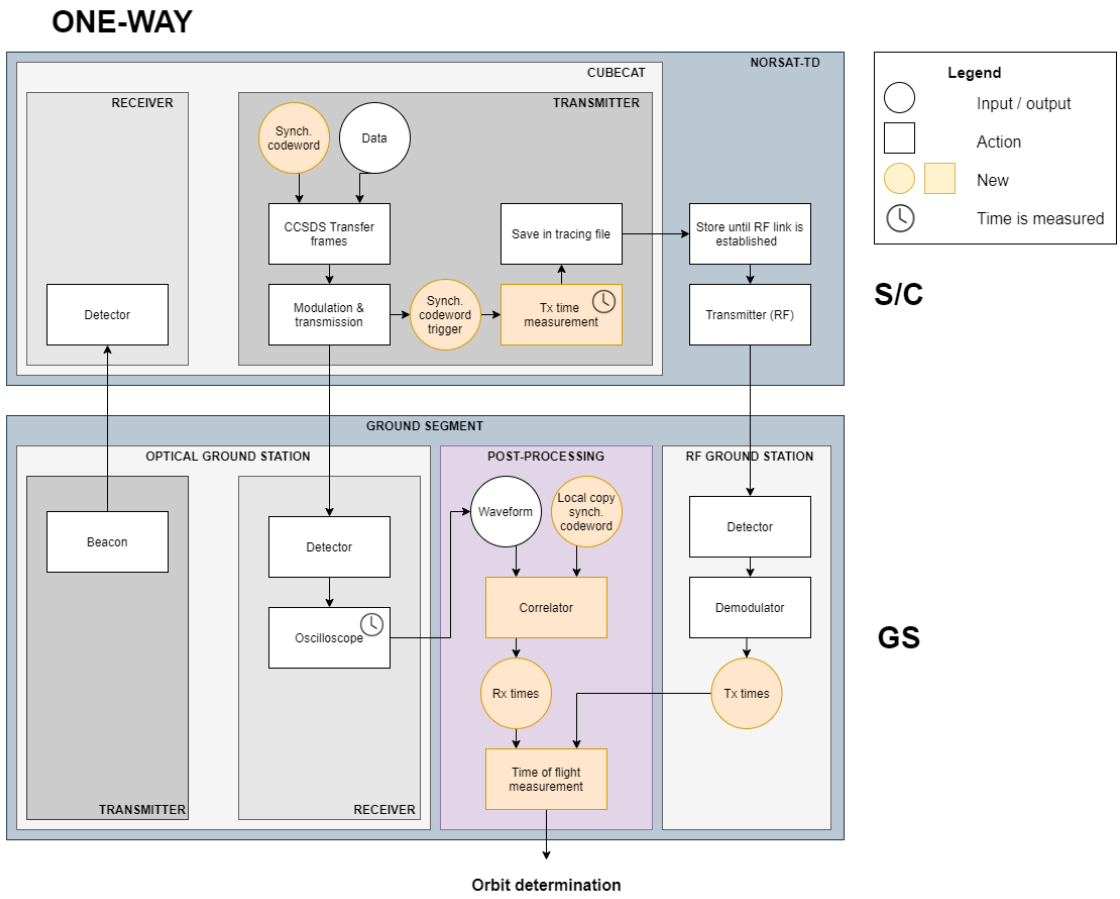

Figure 4.10: One-way telemetry-based ranging block diagram.

4.3.2. Long-term outlook: two-way ranging

On the long-term, there could be a possibility to incorporate two-way ranging as well. An important change should be that the uplink beacon can be modulated. Other changes are dependent on whether the system is two-way synchronous or asynchronous. Similar to one-way ranging, a block diagram was made for the two-way ranging systems. The block diagram for **two-way synchronous** ranging is shown in Figure 4.11. For two-way synchronous ranging, the spacecraft does not have to record timestamps in a tracing file, this is only done at the ground station. The links have to be designed in such a way that the reception of a synchronization codeword marker (CSM) on CubeCat, is synchronized with the transmission of a CSM.

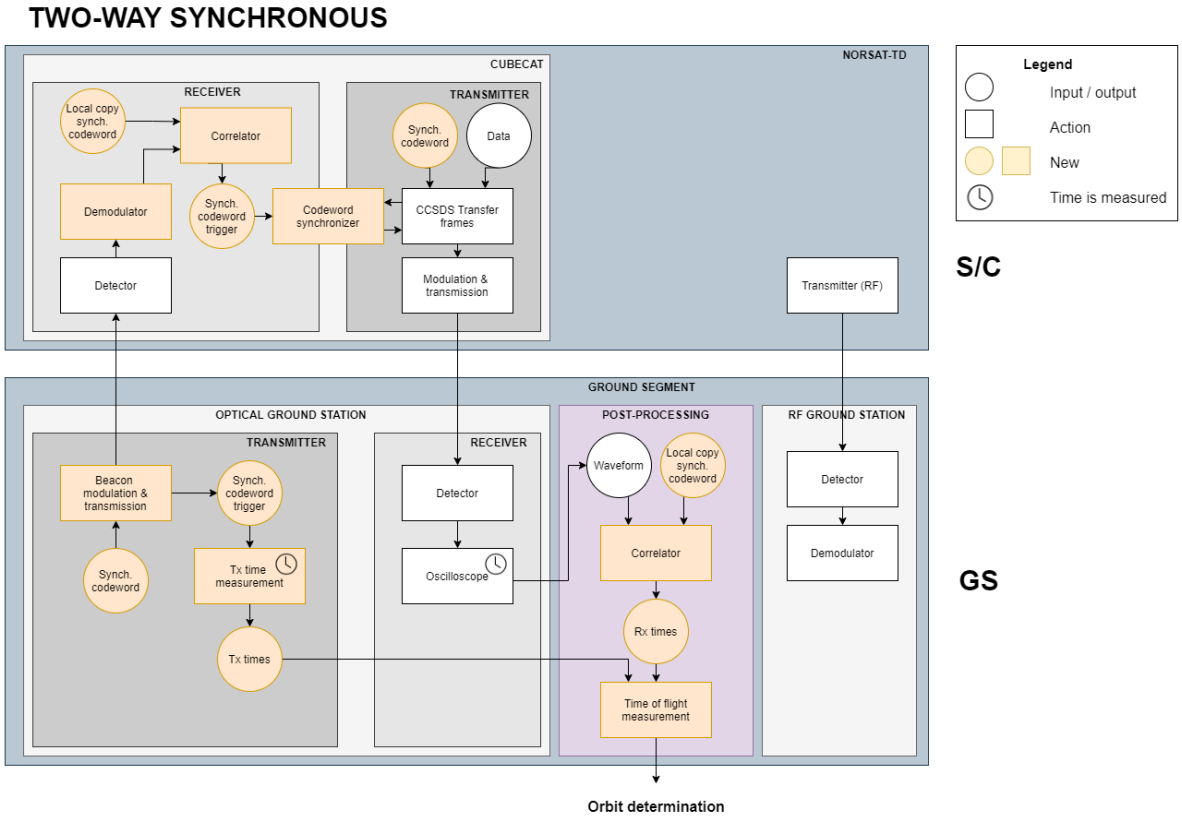

Figure 4.11: Two-way synchronous telemetry-based ranging block diagram.

When comparing this diagram to the one-way diagram in Figure 4.10, it can be concluded that the overall implementation is more impactful because there are more 'new' blocks required on a CubeCat and OGS system level. The new blocks are discussed below:

- Similar to one-way ranging, there is a post-processing block on ground. In subsection 4.3.1 it was already concluded that this post-processing block does not impact CubeCat or the OGS on a system level.
- The transmitter of the OGS shows many new additions because first of all, the beacon has to be modulated with CSM's. Secondly, upon transmission of a CSM, a time measurement has to be made. This is similar to the CubeCat transmitter block in the one-way ranging block diagram. However, it is expected that such a CSM trigger is easier to implement on ground than it is on CubeCat.
- At CubeCat's receiver, a demodulator and correlator are placed to create triggers when a CSM arrives. This trigger is sent to a codeword synchronizer which synchronizes the ingoing and outgoing CSM's. This setup is derived from the LLCD codeword synchronizer (Figure 1 in [30]).

From this analysis it can be concluded that a two-way synchronous ranging has more impact on CubeCat and the OGS compared to one-way ranging. Especially additions on CubeCat, such as the correlator and the codeword synchronizer, could make the implementation complex and costly. However, the performance improvement that can be achieved in terms of orbit accuracy make the implementation worth exploring. In

terms of range noise, it was also found that two-way synchronous ranging is most favorable (≈ 3 m) based on the noise budget in subsection 3.3.3, which can be explained by the fact that the T_x and R_x time are measured with the same clock.

The last implementation to be discussed is **two-way asynchronous** ranging. The block diagram for a two-way asynchronous ranging implementation is shown in Figure 4.12. For two-way asynchronous ranging, the spacecraft has to record the timestamps of both the received and transmitted CSM's on the spacecraft. Similar to one-way ranging, this could be achieved with the timestamp tracing capability on CubeCat [34]. Alternatively, only the elapsed time between a received and transmitted synchronization marker could be recorded on CubeCat, so you end up with one time measurement instead of two, which reduces the data storage on the SD card. NASA JPL refers to these kind of measurements as phase measurements [28].

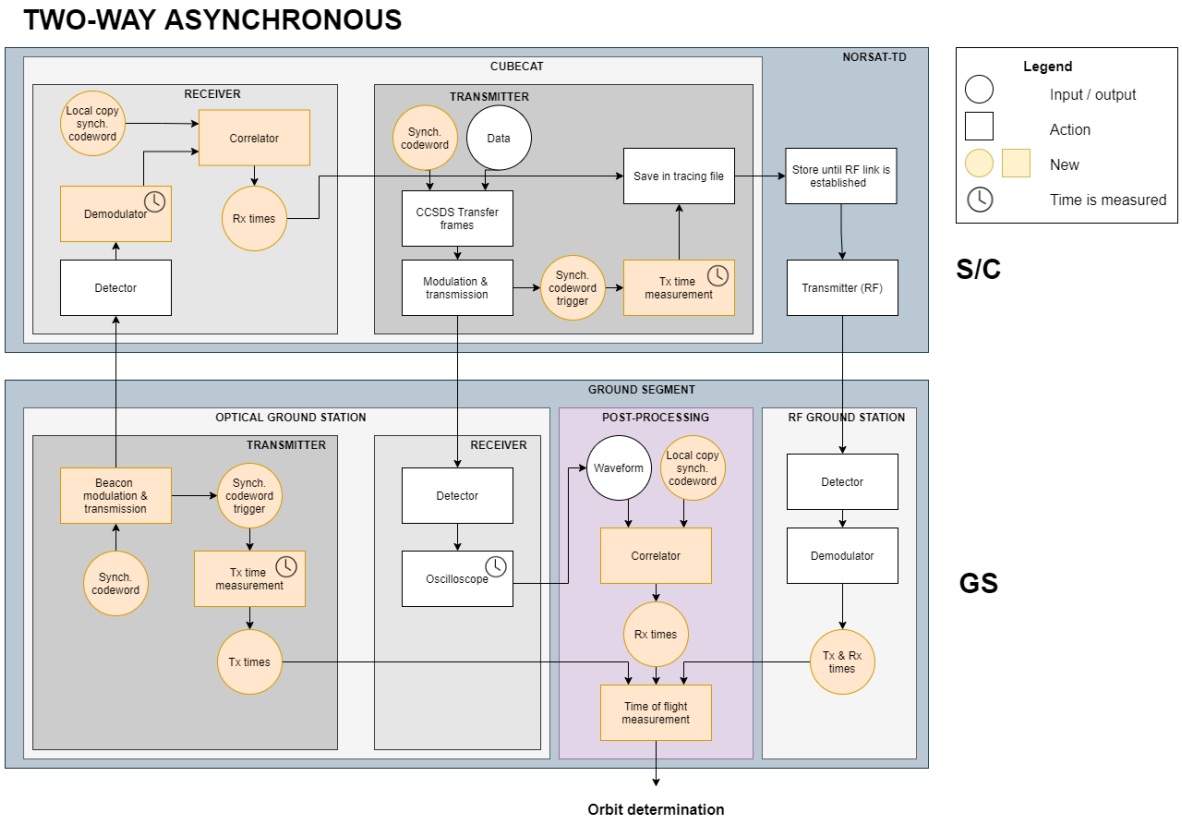

Figure 4.12: Two-way asynchronous telemetry-based ranging block diagram.

The right side of the block diagram is almost identical to the one-way ranging block diagram, while the left side shows more similarities with the two-way synchronous diagram. The main difference with the latter is that there is no connection between the incoming and outgoing timestamps on the spacecraft. In other words, the uplink and downlink are independent from each other. A brief overview of the most important 'new' blocks:

- Similar to the previous two diagrams, there is a post-processing block on ground. Main difference is that the TOF measurement is constructed from four timestamps (i.e. two one-way ranges) instead of two timestamps.
- The transmitter block of the OGS is identical to the one in the two-way synchronous block diagram in Figure 4.11.
- Also the receiver block on CubeCat is similar to the two-way synchronous diagram. The main difference is the output of the correlator. For two-way synchronous ranging the output of the correlator was a trigger to the codeword synchronizer. In this diagram the output is an R_x time measurement which is saved in the tracing file in a similar fashion as the T_x measurements.

- The transmitter block on CubeCat is identical to the one in the one-way diagram. In general it can be observed that the uplink and downlink flow in two-way asynchronous ranging is largely similar. It is expected that this will be easier to implement than a synchronizer.

To summarize, it can be concluded that the two-way ranging systems are advantageous in terms of ranging performance while the one-way system is more favorable in terms of implementation because it requires the least amount of adjustments. It can be argued that the two-way asynchronous implementation is a more logical iteration of the one-way implementation than two-way synchronous ranging because the uplink and downlink flow are largely similar. However, two-way synchronous ranging is favorable over asynchronous ranging in terms of range noise (≈ 3 m versus ≈ 17 m).

5

Conclusion

The aim of the thesis project was to investigate the possibility of laser ranging with the laser communication terminal CubeCat and the TNO OGS. Laser ranging and communication can be combined through telemetry-based ranging which basically makes the range measurement a byproduct of the laser communication data [16][28]. Telemetry-based ranging is described by NASA JPL with a focus on compatibility with the CCSDS optical standards [6][7]. However, the CCSDS optical standards and the NASA JPL research were written in the context of high-photon efficient systems and not for O3K (CubeCat's modulation scheme). The CCSDS is aware of a growing interest from the industry in O3K for less complex near-Earth applications such as cube-sats. The CCSDS working group is therefore in the process of expanding the optical standards for O3K [13]. An implementation on CubeCat and the TNO OGS would be a stepping stone towards this standardization.

The concept of telemetry-based ranging originates from the radio frequency domain [28]. Attempts of telemetry ranging in the optical domain so far are limited. The most successful attempt was made during the LLCD on LADEE where centimeter level range noise was reached [30]. For the feasibility study on telemetry-based ranging with O3K encoded data, a correlation model was created, as described in section 2.2, which correlates the received signal with a code synchronization marker (CSM) to obtain a time delay which is equal to a time of flight measurement in traditional ranging. The correlation model was subjected to a test data set to investigate the correlation ambiguity and induced range noise. To resolve the ambiguity of identifying the correlation peak, as described in subsection 2.3.1 and 4.1, a correlation or CSM size of at least 64 bits was recommended. This is a little bit more than the required bit-length of 48 bits for 4-PPM described by the CCSDS optical standard [6]. The precision of this technique was initially found to be limited by the temporal resolution of the received data. However, by letting the correlator integrate over a longer period of time (i.e. using a larger CSM), the temporal resolution induced noise can be reduced to jitter level [3]. The required minimum CSM length was calculated analytically with Equation 2.2 in subsection 2.3.2. Based on this input it was determined an uplink of 200 kbps required a 512-bit synchronization marker and a downlink of 100 Mbps required a 128-bit synchronization marker. The maximum downlink data rate reduction resulted in 3% with a timestamp tracing rate of 20 kHz.

After the analysis of the telemetry-based correlation technique, it was investigated in which ranging configuration it could be applied. The three main ranging system options were: one-way, two-way synchronous and two-way asynchronous ranging. Through a clock error analysis it was found that one-way ranging contains an accumulating time-correlated error caused by the bias and bias instabilities of two different clocks [12]. The time-correlated error can be modeled with a second order polynomial, as described by Equation 3.8 in section 3.2, over short clock arcs. For the two-way ranging systems the approach is much simpler as the clock error can be modeled as a constant and a random noise. The orbit estimation strategies for each ranging system was evaluated with a covariance analysis in which the formal errors and correlations were analysed. It was found that adding many clock parameters complicates the isolation of the range signal from the range noise in the estimation. As a result the crosscorrelations between parameters and the formal errors increased up till a point where the inverse covariance matrix ($H^T W H$) became singular. To prevent singularity apriori information was applied on the state and clock parameters. The most representative clock arc length is equal to the duration of one pass ($\leq$ 10 min). CubeCat's automated clock synchronization command at the start

(and possibly the end) of each pass provides confidence that apriori information clock information can be accurately determined over this time span [35]. For a 7-day estimation with 4 state arcs with apriori information, a formal position and velocity error of 274 m and 0.4 m/s were found for one-way ranging with clock arcs as short as one pass. This position error is relatively large compared to the formal position errors obtained for two-way ranging which were well below 10 m. This is also an order of magnitude larger than the position error found for one-way application LRO ($\approx$ 30 m) [5].

Besides the impact of clock arcs and apriori information it was also investigated what the impact of range noise was. In subsection 3.3.3, the expected range noise was analysed for each of the three ranging systems. A range noise value of 12 m, 3 m and 17 m was estimated for one-way, two-way synchronous and two-way asynchronous ranging between CubeCat and the OGS respectively. This is relatively large compared to the centimeter noise floor of the LLCD measurements. However, the centimeter-level noise of the LLCD are a result of pre-processing the raw range measurements through averaging [30]. This is also a recommended approach for TOF measurements from CubeCat and the OGS. The main cause for the meter-level noise estimates is the expected GPS clock precision on cubesats which is currently set to 40 ns based on commercially available products. A more elaborate analysis on CubeCat's clock and timing performance is required to assign a more accurate value to this particular noise source (see recommendations) but it is expected that this value will at least be in the same order of magnitude as the current estimate. In subsection 3.3.5 and 4.2 it was concluded that the formal errors increase linearly with range noise, and thus noise has a significant impact. This means that if the one-way range noise could be reduced to e.g. 1 m, the 274 m formal position error with clock arcs per pass would be reduced to approximately 23 m, which would be similar to LRO's orbit accuracy [5].

The last test case that was investigated was the impact of having two additional ground stations available that can provide one-way range measurements. It was found that this addition smoothed the stronger crosscorrelations between state and clock parameters, but that it also increased some other crosscorrelations. This was caused by the additional clock arcs needed for the observations of these two extra ground stations. However, the overall improvement was clearly noticeable as the 274 m and 0.4 m/s formal position and velocity error decreased to 105 m and 0.1 m/s. Although the current setup consists of only one ground station, namely the TNO OGS, it could be worth to explore combined laser ranging and communication with a ground station network in the future. As a final note on the covariance analysis, although the formal errors are expected to be near the true errors, there are certain aspects that should be taken into account which could possibly lead to higher true errors, as described in section 4.2. Formal errors may differ from the true errors when dynamics are not modelled correctly or when the observation noise is incorrectly quantified. In addition, time-correlated noise artifacts could be found over time spans shorter than a pass (< 10 min), but it is uncertain whether these artifacts are strong enough to impact the true errors.

Based on the formal error analysis it could be concluded that two-way ranging has a significant advantage over one-way ranging. However, this advantage was put into perspective when comparing the practical implementation of telemetry-based ranging for these three ranging systems on CubeCat and the TNO OGS, as described and visualized in section 4.3. From an implementation perspective, it could actually be concluded that a one-way implementation requires the least amount of changes. The main changes that a two-way implementation requires is a beacon at the OGS that can be modulated and a correlator on the spacecraft, as shown in Figure 4.11 and 4.12. These required changes make a two-way implementation currently infeasible for the CubeCat that is being developed right now but future iterations could take these requirements into account. One-way ranging is therefore the only feasible option for a combined laser ranging and communication implementation on a short-term. Although it is expected that one-way telemetry-based ranging will not result in highly accurate orbit solutions, the implementation itself would already be a valuable demonstration of combined laser ranging and communication for future iterations of CubeCat, as well as a contribution to the standardization of telemetry-based ranging with O3K compatibility.

6

Recommendation

Five main recommendations for future work on combined laser ranging and communication between CubeCat and the TNO OGS were identified. These recommendations concern (1) the O3K test data, (2) the clock noise analysis, (3) noise reduction through time averaging, (4) future CCSDS developments, and (5) a hybrid form of telemetry ranging. The O3K oscilloscope test data set that was used during this study was verified as a representative data set for a preliminary analysis on the feasibility of O3K telemetry ranging. Dominant factors that impact the performance of the correlation technique such as correlation size, temporal resolution and SNR have been addressed. However, smaller factors such as rise time, jitter and communication interruptions due to atmospheric fading have not been quantitatively assessed. To gain more confidence in the overall feasibility of telemetry-based ranging with O3K, it is recommended to assess these less dominant factors as well. This can be done by generating oscilloscope data that matches the expected signal more closely in terms of data rate, rise time and jitter, or by using actual laser communication data from a representative LEO satellite such as SOCRATES[1], AeroCube[2] or PIXL-1[3].

In line with the previous recommendation on confidence improvement is the following recommendation on the clock noise analysis. The clock noise analysis, as presented in subsection 3.3.3, was based on available information on CubeCat and the TNO OGS. Missing noise sources were quantified based on literature and commercially available hardware. Since it was observed that range noise scales linearly with the formal errors, it is worthwhile to support the noise budget with clock tests on the actual hardware. More confidence in the noise budget will lead to more confidence that the true errors will be close to the formal errors. The third recommendation suggests an additional improvement of the range noise. As described in subsection 3.3.3, the LLCD was able to reduce the range noise in its measurements through averaging over 1 s periods [30]. Traditional ranging is often bound to 0.5 s observation intervals to resolve range ambiguity [28]. Telemetry-based ranging however, allows for smaller intervals. For orbit determination purposes these additional range measurements are not required because they do not add substantial new information in the H-matrix to make a significant difference in the orbit error. These additional range measurements can therefore be considered as redundant and could be used to remove some of the dominant noise sources through averaging before the orbit determination process.

The fourth recommendation concerns CCSDS developments. As mentioned earlier in the report, there is ongoing development regarding the CCSDS optical standards. The CCSDS working group acknowledges a growing interest from the industry for low-complexity optical systems with OOK encoding [13]. A call for proposals has opened that should lead to O3K and one-way ranging solutions for CCSDS telemetry-based ranging. It is important that in future studies on combined laser ranging and communication, CCSDS developments are followed closely to prevent any 'reinvention of the wheel' and possible compatibility issues in the future. The fifth and last recommendation is on a hybrid form of telemetry ranging. This would include an RF uplink and an optical downlink. Theoretically, this could actually be a two-way ranging solution for the current CubeCat. However, there are two main aspects that complicate such a solution. First of all, the RF

[1] SOCRATES:https://directory.eoportal.org/web/eoportal/satellite-missions/content/-/article/socrates
[2] AeroCube: https://directory.eoportal.org/web/eoportal/satellite-missions/a/aerocube-ocsd
[3] PIXL-1: https://eoportal.org/web/eoportal/satellite-missions/content/-/article/pixl-1

ground station will be located somewhere else than the optical ground station. It is therefore likely that the RF uplink and optical downlink occur in separate time windows which makes it impossible to combine the individual ranges into a two-way range. Secondly, the RF subsystem is part of NorSat-TD [35]. Since CubeCat is a plug-and-play demonstration payload, it is unlikely that the NorSat-TD RF link can be integrated with CubeCat's optical downlink. A study focused on the electrotechnical side of CubeCat could potentially offer solutions on hybrid forms of telemetry-based ranging for future iterations of CubeCat.

A

Additional information on CubeCat and the optical ground station

This appendix provides additional information on CubeCat and the OGS. Section A.1 contains specifications of CubeCat and the TNO OGS. Note that these specifications are confidential. Section A.2 provides an overview of link budget calculations and the link budget itself. The information in this appendix is not part of the core of the thesis study but is meant to provide additional background information to readers who wish to learn more about CubeCat and the TNO OGS.

A.1. Specifications

Section A.1 is confidential and therefore removed from this public version of the report. Please contact the author to request access.

A.2. Links

This appendix describes how the link budget was calculated. Subsection A.2.1 gives an overview of all the relevant equations and subsection A.2.2 presents the link budget itself including a description of the most significant parameters.

A.2.1. Link equations

The power at the receiving aperture is dependent on the transmitted power, gains, and losses, as shown in Equation A.1 [10][23].

$$P_R = P_T G_T L_T L_P L_{FS} L_{ATM} L_{SR} L_{SI} L_{BW} G_R L_R \tag{A.1}$$

From left to right: P_R R_x power, P_T T_x power, G_T T_x gain, L_T T_x optical loss, L_P pointing loss, L_{FS} free-space loss, L_{ATM} atmospheric attenuation, L_{SR} Strehl-ratio loss, L_{SI} scintillation loss, L_{BW} beam wander loss, G_R R_x gain, L_R R_x optical loss. When the half divergence angle $\theta_{1/2}$ is known the T_x gain can be calculated as follows [9]:

$$G_T = \frac{8}{\theta_{1/2}^2} \tag{A.2}$$

The R_x gain is dependent on the receiving aperture D_R, wavelength λ, and obscuration ratio γ (if a secondary mirror is used), as shown in Equation A.3 [23]. The latter parameter is applicable to the Ritchey-Chrétien telescope of the TNO ground station. If no secondary mirror is present, the obscuration ratio is simply zero.

$$G_R = \left(\frac{\pi D_R}{\lambda}\right)^2 (1-\gamma^2) \tag{A.3}$$

The optical efficiency losses L_T and L_R were assumed to be 0.7 and 0.85 respectively which are a typical values [23]. The pointing loss L_P is dependent on the ratio between the pointing error θ_P and the half divergence angle $\theta_{1/2}$ according to the following equation [9]:

$$L_P = \exp\left[-2\left(\frac{\theta_P}{\theta_{1/2}}\right)^2\right] \tag{A.4}$$

The free-space loss is dependent on the wavelength and the distance d over which the signal travels. For a worst-case estimation one should use the distance at lowest elevation which is equal to the maximum distance. The loss is calculated as follows [23]:

$$L_{FS} = \left(\frac{\lambda}{4\pi d}\right)^2 \tag{A.5}$$

The maximum atmospheric attenuation L_{ATM} was provided by TNO [34]. The Strehl-ratio loss L_{SR} for closed-loop tracking control was determined with [4]:

$$L_{SR} = \left[1 + \left(5.56 - \frac{4.84}{1+0.04(W_0/r_0)^{5/3}}\right)\cdot (W_0/r_0)^{5/3}\right]^{-6/5} \tag{A.6}$$

Where W_0 is the beam width at $1/e^2$ intensity, and r_0 is the atmospheric coherence length also known as the Fried parameter. The scintillation loss L_{SI} is dependent on the scintillation index SI and the outage probability p, as shown in Equation A.7 [10]. The scintillation index is in turn dependent on beam width, wavelength, link distance, the Fried parameter r_0, and the zenith angle [15].

$$L_{SI} = \left(3.3 - 5.77\sqrt{\ln\left(\frac{1}{p_{out}}\right)}\right)\cdot SI^{4/5} \tag{A.7}$$

Lastly, the beam wander $< r_c^2 >$ was determined with the beam width, the altitude difference between transmitter and receiver $(H-h_0)$, Fried parameter and zenith angle ζ as follows [4]:

$$< r_c^2 >= 0.54(H-h_0)^2 \sec^2(\zeta)\left(\frac{\lambda}{2W_0}\right)^2\left(\frac{2W_0}{r_0}\right)^{5/3} \tag{A.8}$$

From which the beam wander angle θ_{BW} follows [4]:

$$\theta_{BW} = \frac{\sqrt{< r_c^2 >}}{d} \tag{A.9}$$

By inserting the beam wander angle in Equation A.4, the beam wander loss can be determined with the divergence angle. Beam wander loss for the downlink was assumed to be zero because the beam width has diverged long enough before it encounters strong turbulence. Equation A.8 decreases with an increasing W and thus L_{BW} is assumed to be negligible for the downlink.

A.2.2. Link budget

A link budget was set up to determine the required T_x power to achieve the minimum irradiance at either end of the link. The link budget, as shown in Table A.1, was calculated at minimum elevation, maximum slant range and clear sky conditions. The formulae and assumptions that were used to determine the link budget parameters were described in section A.2 and all the relevant input values were given in section A.1. Note that this budget is based on a tracking phase. During an acquisition phase, the pointing loss is expected to be higher. The losses L_{SR}, L_{SI} and L_{BW} were merged into one atmospheric turbulence loss L_{TUR} for clarity.

Table A.1: Link budget TNO OGS - CubeCat.

Parameter		**Uplink**		**Downlink**	
P_T	T_x power	15	W	0.3	W
		41.8	dBm	24.8	dBm
G_T	T_x gain	83.0	dB	91.0	dB
L_T	T_x optical loss	-1.5	dB	-1.5	dB
L_P	Pointing loss	-0.1	dB	-4.9	dB
L_{ATM}	Atmospheric attenuation	-0.5	dB	-0.5	dB
L_{FS}	Free space loss	-258.0	dB	-258.2	dB
L_{TUR}	Atmospheric turbulence loss	-8.8	dB	-4.5	dB
G_R	R_x gain	89.4	dB	123.5	dB
L_R	R_x optical loss	-0.7	dB	-0.7	dB
P_R	**R_x power expected**	**2.9**	**nW**	**792**	**nW**
		-55.3	**dBm**	**-31.0**	**dBm**
P_{REQ}	**R_x power required**	**1.4**	**nW**	**754**	**nW**
		-58.5	**dBm**	**-31.2**	**dBm**
	Margin	3.2	dB	0.2	dB

From Table A.1 it can be observed that quite a bit more power is required for the uplink compared to the downlink. A few parameters that have the most significant contribution to this difference:

- G_T: The divergence angle of the OGS's beacon is 2.5 times smaller than CubeCat's divergence angle. G_T increases with the squared inverse of the half divergence angle which explains the difference.
- L_{TUR}: Differences in scintillation losses are caused by the difference in receiver apertures. A smaller aperture leads to a higher scintillation index and thus scintillation loss.
- G_R: This where the large telescope aperture of the OGS makes the most significant contribution.

Bibliography

[1] Abshire, J., Gardner, C. Atmospheric refractivity corrections in satellite laser ranging. *Geoscience and Remote Sensing, IEEE Transactions on*, 23:414 – 425, 1985. doi: 10.1109/TGRS.1985.289431.

[2] Agrawal, G.P. *Fiber-optic Communication Systems*. Microwave and Optical Engineering. John Wiley & Sons, Inc., 4th edition, 2010.

[3] Andrews, K., Hamkins, J., Shambayati, S., Vilnrotter, V. Telemetry-based ranging. *IEEE Aerospace Conference Proceedings*, 01 2011. doi: 10.1109/AERO.2010.5446926.

[4] Andrews, L.C., Phillips,R.L., Sasiela, R.J., Parenti, R.R. Strehl ratio and scintillation theory for uplink Gaussian-beam waves: beam wander effects. *Optical Engineering*, 45(7):1 – 12, 2006. doi: 10.1117/1.2219470.

[5] Bauer, S., Hussmann, H., Oberst, J., Dirkx, D., Mao, D., Neumann, G.A., Mazarico, E., Torrence, M.H., McGarry, J.F., Smith, D.E., Zuber, M.T. Demonstration of orbit determination for the Lunar Reconnaissance Orbiter using one-way laser ranging data. *Planetary and Space Science*, Volume 129:32–46, 2016.

[6] Consultative Committee for Space Data Systems. CCSDS recommended standard for optical communications coding and synchronization (Blue book 142.0-B-1), 2019.

[7] Consultative Committee for Space Data Systems. CCSDS recommended standard for optical communications physical layer (Blue book 141.0-B-1), 2019.

[8] Consultative Committee for Space Data Systems. CCSDS draft recommended standard for optical communications physical layer (Pink sheets 141.0-P-1.1), 2020.

[9] Degnan, J.J. Millimeter Accuracy Satellite Laser Ranging: A Review. *Contributions of Space Geodesy to Geodynamics: Technology*, Geodynamics Series Volume 25:133–162, 1993.

[10] Dimitrov, S., Barrios, R., Matuz, B., Liva, G., Mata-Calvo, R., Giggenbach, D. Digital modulation and coding for satellite optical feeder links with pre-distortion adaptive optics'. *International Journal of Satellite Communications and Networking*, 34:625–644, 2015.

[11] Dirkx, D. *Interplanetary Laser Ranging: Analysis for Implementation of Planetary Science Missions*. PhD thesis, Delft University of Technology, 2015.

[12] Dirkx, D., Noomen, R., Visser, P.N.A.M., Bauer, S., Vermeersen, L.L.A. Comparative analysis of one- and two-way planetary laser ranging concepts. *Planetary and Space Science*, 117:159–176, 2015. ISSN 0032-0633. doi: https://doi.org/10.1016/j.pss.2015.06.005.

[13] Edwards, B., Daddato, R., Schulz, K., Alliss, ., Hamkins, J., Giggenbach, D., Robinson, B., Braatz, L. An Update on the CCSDS Optical Communications Working Group Interoperability Standards. pages 1–9, 2019. doi: 10.1109/ICSOS45490.2019.8978979.

[14] Geul, J., Mooij, E., Noomen, R. TLE Uncertainty Estimation using Robust Weighted Differencing. *Advances in Space Research*, 2017. doi: 10.1016/j.asr.2017.02.038.

[15] Giggenbach, D., Henniger, H. Fading-loss assessment in atmospheric free-space optical communication links with on-off keying. *Optical Engineering*, 47:046001–1, 2008. doi: 10.1117/1.2951952.

[16] Hamkins, J., Kinman, P., Xie, H., Vilnrotter, V., Dolinar, S. Telemtry Ranging: Concepts. *The Interplanetary Network Progress Report*, vol. 42-203:1–20, 2015.

[17] Hampf, D., Schafer, E., Sproll, F., Otsubo, T., Wagner, P., Riede, W. Satellite Laser Ranging at 100 kHz Pulse Repetition Rate. *CEAS Space Journal*, 11, 2019. doi: 10.1007/s12567-019-00247-x.

[18] Hemmati, H. Interplanetary laser communications and precision ranging. *Laser Photonics Reviews*, Volume 5:697–710, 2011.

[19] Hennawy, J.R., Adams, N., Erika A., Sanchez, E.A., Srinivasan, D., Hamkins, J., Vilnrotter, V., Xie, H., Kinman, P. Telemetry ranging using software-defined radios. *2015 IEEE Aerospace Conference*, pages 1–14, 2015.

[20] Hyperion Technologies B.V. CubeCat: Laser Communication Terminal, 2019.

[21] Iraci, G., Gnam, C. An Open Source Radio for Low Cost Small Satellite Ranging. University of Buffalo Nanosatellite Laboratory, 2018.

[22] Jensen, J.R., Haskins, C.B., DeBoy, C.C. Regenerative PN ranging experience with New Horizons during 2012. In *2013 IEEE Aerospace Conference*, pages 1–7, 2013. doi: 10.1109/AERO.2013.6496983.

[23] Kaushal, H., Jain, V.K., Kar, S. *Free Space Optical Communication*. Optical Networks. Springer (India) Pvt. Ltd., 1st edition, 2017.

[24] Majid, A., Owais, M.N., Qureshi, M.N. Aerodynamic Drag Computation of Lower Earth Orbit (LEO) Satellites. *Journal of Space Technology*, Volume 8, 2018.

[25] Montenbruck, O., Gill, E. *Satellite Orbits: Models, Methods, and Applications*. Springer, 2nd edition, 2001.

[26] Rose, T.S., Rowen, D.W., LaLumondiere, S., Werner, N.I., Linares, R., Faler, A., Wicker, J., Coffman, C.M., Maul, G.A., Chien, D.H., Utter, A., Welle, R.P., Janson, S.W. Optical communications downlink from a 1.5U Cubesat: OCSD program. In *International Conference on Space Optics — ICSO 2018*, volume 11180.

[27] Saathof, R., Crowcombe, W., Kuiper, S., van der Valk, N., Pettazzi, F., de Lange, D., Kerkhof, P., van Riel, M., de Man, H., Truyens, N., Ferrario, I. Optical Satellite Communication Space Terminal Technology at TNO. In *International Conference on Space Optics*. TNO Technical Sciences, 2018.

[28] Sanchez, M., Hamkins, J. Optical Telemetry Ranging. *The Interplanetary Network Progress Report*, vol. 42-221, 2020.

[29] Smith, D.E., Zuber, M.T., Sun, X., Neumann, G.A., Cavanaugh, J.F., McGarry, J.F., Zagwodzki, T.W. Two-Way Laser Link over Interplanetary Distance. *Science*, Volume 311:53, 2006.

[30] Stevens, M.L., Parenti, R.R., Willis, M.M., Greco, J.A., Khatri, F.I., Robinson, B.S., Boroson, D.M. The lunar laser communication demonstration time-of-flight measurement system: overview, on-orbit performance, and ranging analysis. In *Free-Space Laser Communication and Atmospheric Propagation XXVIII*, volume 9739, pages 48 – 59. International Society for Optics and Photonics, SPIE, 2016. doi: 10.1117/12.2218624.

[31] Sun, X., Skillman, D.R., Hoffman, E.D., Meo, D., McGarry, J.F., et al. Simultaneous laser ranging and communication from an Earth-based satellite laser ranging station to the Lunar Reconnaissance Orbiter in lunar orbit. In *Free-Space Laser Communication and Atmospheric Propagation XXV*. NASA Goddard Space Flight Center, 2013.

[32] Sweeting, M. Modern Small Satellites-Changing the Economics of Space. *Proceedings of the IEEE*, 106: 343–, 2018. doi: 10.1109/JPROC.2018.2806218.

[33] TNO. OCL-TN-TNO-TEL-0001. Confidential unpublished document, 2019.

[34] TNO. CCAT-TNO-ST-ICD-0001. Confidential unpublished document, 2020.

[35] TNO. CCAT-TNO-ST-TN-0008. Confidential unpublished document, 2021.

[36] u-blox. GPS-based Timing: Considerations with u-blox 6 GPS receivers. Application note, 2011.

[37] Vallado, D., Cefola, P. Two-line element sets - Practice and use. *Proceedings of the International Astronautical Congress, IAC*, 7:5812–5825, 2012.

[38] Xue, Z., Charonko, J.J., Vlachos, P.P. Signal-to-noise ratio, error and uncertainty of PIV measurement. In *PIV13; 10th International Symposium on Particle Image Velocimetry*. Virginia Tech, 2013.